Journal of Building Engineering 127 (2026) 116374

Contents lists available at ScienceDirect

Journal of Building Engineering

journal homepage: www.elsevier.com/locate/jobe

Fayalite slag and municipal solid waste incineration bottom ash as sand replacement in cement mortar: Physical, mechanical, and durability properties

Adeolu Adediran [a,*], Nana Asaam [a], Javier Manso-Morato [a,b], Erdi Avci [a,c], Priyadharshini Perumal [a]

[a] Fibre and Particle Engineering Research Unit, University of Oulu, Pentti Kaiteran katu 1, 90014, Oulu, Finland
[b] Department of Civil Engineering, Escuela Politécnica Superior, University of Burgos, c/Villadiego s/n, 09001, Burgos, Spain
[c] Department of Geological Engineering, İstanbul University-Cerrahpaşa, İstanbul, 34500, Türkiye

ARTICLE INFO

Keywords:
Fayalite slag
Bottom ash
Cement mortar
Alkali–silica reaction
Freeze-thaw
Sulfate and chloride
Construction application

ABSTRACT

Approximately 300,000 tons of municipal solid waste incineration bottom ash (BA) and 600,000 tons of fayalite slag (FS) are generated annually in Finland from metallurgical and incineration processes, with the majority of them disposed of in landfills or used in low-value applications. This study investigated the potential upcycling of FS and BA as sand replacements in cement-based mortars to avoid landfilling, conserve natural resources, and ensure efficient use of industrial residues. Standard sand (SS) was used as the main fine aggregate. The effect of replacing SS partly or wholly with either FS or BA was investigated through workability, compressive strength, ultrasonic pulse velocity (UPV), scanning electron microscope analysis, capillary water absorption, alkali–silica reaction (ASR), freeze-thaw cycles in water, and combined sodium sulfate and sodium chloride solution exposure. The aggregates' leaching results were below the values stipulated by Finnish and EU regulations. Partial or full replacement of SS with either FS or BA resulted in lower workability. Full replacement of SS with FS resulted in comparable properties to the reference mix in terms of compressive strength, UPV, and capillary water absorption. Meanwhile, partial replacement of SS with FS resulted in higher compressive strength and UPV but reduced water absorption. In contrast, partial or full replacement of SS with BA resulted in lower compressive strength and UPV, as well as increased water absorption compared with the reference mix. All samples remained stable after exposure to freeze-thaw cycles in water. However, only the reference samples and samples containing 50% replacement of SS with either FS or BA were stable after exposure to freeze-thaw cycles in a combined sulfate and chloride solution, whereas those containing 100% FS or BA were completely degraded. Of all the aggregates, only FS satisfied the 14-day ASR requirements according to the ASTM C1260 standard, achieving a low expansion rate of 0.009%.

1. Introduction

Concrete is one of the most widely used materials worldwide. Meanwhile, the production and usage of concrete have continued to

* Corresponding author.
E-mail address: adeolu.adediran@oulu.fi (A. Adediran).

https://doi.org/10.1016/j.jobe.2026.116374
Received 31 January 2026; Received in revised form 11 May 2026; Accepted 21 May 2026
Available online 22 May 2026

increase due to the demand for buildings and infrastructure development around the world, which is estimated to reach approximately 18 billion tons annually by 2050 [1–3]. The main solid components of mortar and concrete, namely Portland cement (PC) and natural aggregates, have continued to experience an astronomical increase in demand. Currently, the production of PC is responsible for 7%–9% of global anthropogenic carbon emissions [4–6]. Similarly, the extensive and uncontrolled extraction of natural aggregates for construction has resulted in severe environmental degradation, such as increased erosion, river salinity, and riverbed depths [7]. To reduce the cost and environmental impact of construction materials, research into alternative raw materials that could replace these natural raw materials is of prime importance. The replacement of natural raw materials with eco-friendly secondary raw materials (mainly industrial residues) as aggregates or supplementary cementitious materials in concrete and mortar production is an increasingly adopted approach [8]. In Finland, large amounts of industrial residues are produced annually from various industries, and their suitability as aggregates and binder replacements has been extensively reviewed and reported [2,8]. Meanwhile, fayalite slag (FS) and municipal solid waste incineration bottom ash (BA) are among the most widely produced industrial residues in Finland that remain unexploited and mostly landfilled.

FS is a non-ferrous metallurgy, iron-rich industrial residue produced during copper and nickel extraction [4–6,9,10]. In Finland, an estimated 200,000 tons of water-quenched nickel-based FS and 400,000 tons of slowly cooled copper-based FS are generated annually, with the majority being stored at dumping grounds, resulting in higher landfilling costs for the producing companies. Several strategies have been developed to minimize their disposal and encourage their reuse as construction materials [6,11,12]. Notably, FS possesses physical, chemical, and mineralogical characteristics that make it suitable for partial or total replacement of aggregates in mortars. For instance, FS is available in granular form due to water quenching, with particle sizes ranging from 0 to 2 mm. Therefore, FS can be used as a fine aggregate because it has a suitable particle size for mortar sand replacement [4–6,9]. Chemically, FS consists of Fe_2O_3 and SiO_2 with lower amounts of Al_2O_3 and CaO [4–6,9]. Mineralogically, FS is mostly associated with fayalite, and magnetite, with lower amorphous content [10]. Furthermore, FS exhibits favorable technical and mechanical properties, such as excellent soundness, good abrasion resistance, and stability. These properties make it suitable as an excellent alternative aggregate for the construction industry. Due to these properties, several researchers have investigated the effects of replacing natural sand with FS from copper production on the mechanical and durability properties of cement-based mortars cured at room temperature (≈20 °C) and the results were promising [11,13–15]. For example, some studies reported an increase in the compressive strength of mortar and concrete when sand was replaced with 20%–100% FS, with the highest strength observed in mortar samples containing 50% FS and 50% sand [11,16,17]. Other studies have shown that replacing sand with 10%–50% FS can increase the 7- and 28-day compressive strengths of high-performance and normal concrete, beyond which the compressive strength starts to decrease, with concrete containing 100% FS having lower compressive strength than the reference samples [11,13,18]. Furthermore, other studies have reported an increase in the strength and durability of high-strength concrete when FS replaces less than 40% of the sand [19–22].

BA is another secondary raw material with a high potential to be used as an alternative aggregate but with a low usage fraction. BA is an industrial residue produced during the incineration of municipal solid waste [23,24]. The amount of BA produced annually has continued to increase due to the growing population and the amount of municipal solid waste generated, estimated at 20 million tons annually in Europe [23,24]. Approximately 300,000 tons of BA are produced annually in Finland, with over 90% being landfilled or used in low-value applications [23,24]. Several use pathways have been proposed and explored to avoid landfilling and ensure compliance with the EU directive on zero waste, principally through upcycling as construction materials. BA is available in granular form, with particle sizes ranging from 0 to 2 mm [24]. BA is rich in SiO_2, Al_2O_3, and CaO [24]. In terms of mineralogy, BA comprises anorthite, anorthoclase, quartz, orthoclase, and calcite as the main crystalline phases [24]. BA has been considered a potential raw material for lower structural layers of road and field structures and other construction applications due to its physical, chemical, and mineralogical properties [24–26]. Despite this, a large fraction of BA remains unexplored. The effects of replacing natural sand with BA on the mechanical and durability properties of cement-based mortars have been investigated by several researchers. Most studies in the literature have reported that the use of BA as aggregate in mortars and concrete can negatively affect the material's mechanical and microstructural properties [27–35]. Vaitkus et al. [27] investigated the properties of BA and its potential suitability as an aggregate replacement in road building materials. Polozhiy et al. [28] investigated the feasibility of replacing sand with BA as a fine aggregate in concrete and observed that the mechanical and durability properties of the concrete gradually decreased with increasing BA content. Grazulyte et al. [29] observed and reported that the compressive strength of the concrete produced decreased by completely replacing sand with BA. Cheng [30] investigated the replacement of sand with up to 40% BA and assessed the mortar's compressive strength and pore size distribution. In the abovementioned study, cement mortar containing BA as aggregate exhibited higher total and capillary porosity and lower compressive strength than conventional cement mortar containing sand. Tang et al. [31] substituted up to 30% of the sand with BA and investigated its impact on the mechanical performance of the mortar. The compressive strength of all samples decreased with increasing BA content, which was ascribed to the high water absorption of BA, which hindered cement hydration to some degree, resulting in lower compressive strength. BA exhibits higher porosity, lower water absorption, and lower density than sand, which decreases the viscosity, compressive strength, flexural strength, and elastic modulus of cement-based mortars [27–31].

Most studies conducted so far on the use of FS as a fine aggregate in cement mortar have focused on FS from copper production, with limited studies on the use of FS from nickel production. Moreover, the properties of BA and FS can vary from one location to another depending on the source, processing operations, and cooling process. Considering that one of the objectives of this study was to prepare materials encompassing a maximum amount of industrial residues as aggregate replacements, the mechanical and durability properties of cement mortar containing high volumes of BA and FS as aggregates were investigated. The study was conducted according to the following structure: The physical properties of the raw materials were characterized in terms of particle size distribution, particle shape, moisture content, water absorption, dry loose density, and true density. The fresh properties of the mortar samples were characterized in terms of workability, whereas the hardened state properties were evaluated in terms of compressive strength,

ultrasonic pulse velocity (UPV), and capillary water absorption. The durability properties of the mortar samples after exposure to freeze-thaw cycles in water and combined sulfate and chloride solutions were assessed in terms of visual observation, mass loss, and residual compressive strength. In addition, all mortar samples were evaluated for alkali-silica reaction (ASR). The effects of BA and FS as sand replacements on the mortar's microstructure and hydration products were investigated using scanning electron microscopy (SEM) and X-ray diffraction (XRD), respectively.

2. Experimental work

2.1. Materials and methods

CEN standard sand (SS) conforming to the European standard EN 196-1 [36], FS, and BA were used as fine aggregates for the study. SS was used as the reference aggregate. Secondary raw materials, such as BA and FS, were used as alternative aggregates to partially or totally replace SS to reduce reliance on natural aggregates, such as SS. FS is an industrial residue from nickel processing operations, supplied in granular form by Boliden Harjaavalta, Finland. BA is an industrial residue from the incineration of municipal solid waste, supplied in granular form by Oulun Energia, Finland. SS has a particle size distribution (PSD) of 0.08–2.00 mm, maximum moisture content of 0.6% (measured in accordance with the EN 1097-5 standard method [37]), water absorption of 0.2% (measured in accordance with the EN 1097-6 standard method [38]), dry loose density of 1481 kg/m^3, and true density of 2600 kg/m^3. FS has a maximum moisture content of 5.2% (measured in accordance with the EN 1097-5 standard method [37]), water absorption of 0.4% (measured in accordance with the EN 1097-6 standard method [38]), dry loose density of 1851 kg/m^3, and true density of 3800 kg/m^3. Furthermore, BA has a maximum moisture content of 6.6% (measured in accordance with the EN 1097-5 standard method [37]), water absorption of 7% (measured in accordance with the EN 1097-6 standard method [38]), dry loose density of 1581 kg/m^3, and true density of 2800 kg/m^3. FS and BA were dried in an oven at a temperature of 60 °C to achieve a moisture content similar to that of SS. To ensure that all aggregates had a PSD and fineness modulus comparable to those of SS, FS and BA were optimized to obtain a PSD and fineness modulus similar to that of SS (Fig. 1). This was achieved by adjusting different particle size fractions of FS and BA to achieve a PSD range and fineness modulus similar to those of SS.

The shape of the aggregates observed with the aid of an optical microscope shows that SS has a round shape with a smooth surface, whereas FS presents an angular and irregular shape with a rough surface texture. For BA, the aggregates are irregular and angular in shape with a porous surface texture (Fig. 2).

Portland limestone cement (PLC, CEM II 42.5 N) that complies with the EN 197-1 standard [39] was used as the binding material. The PLC has a Blaine surface area of 400 m^2/kg and a density of 3.1 g/cm^3.

The chemical composition of the PLC, coupled with the loss on ignition (LOI) was analyzed using X-ray fluorescence (PANalytical Omnian Axios Max, UK), whereas the density of the raw materials was measured using a helium pycnometer (Micrometrics, USA). A wet module laser diffraction particle size analyzer (LS13320; Beckman Coulter, USA) was used to measure the PSD of PLC after proper dispersion in isopropanol. The median PSD (d_{50}), chemical composition, and density of the PLC are presented in Table 1.

A leaching test was conducted on BA and FS to ascertain their heavy metal concentrations before their use as alternative aggregates in accordance with the EN12457-2 standard [40]. BA and FS were dipped in pure water at a liquid/solid mass ratio of 10 and rotated in a rotary tumbler (Retsch, Germany) for 24 h at 30 rpm. After the rotation was completed, the eluates were collected and analyzed by inductively coupled plasma optical emission spectrometry (ICP-OES) in accordance with the SFS-EN ISO 11885 standard (SFS-EN ISO 11885, 2009).

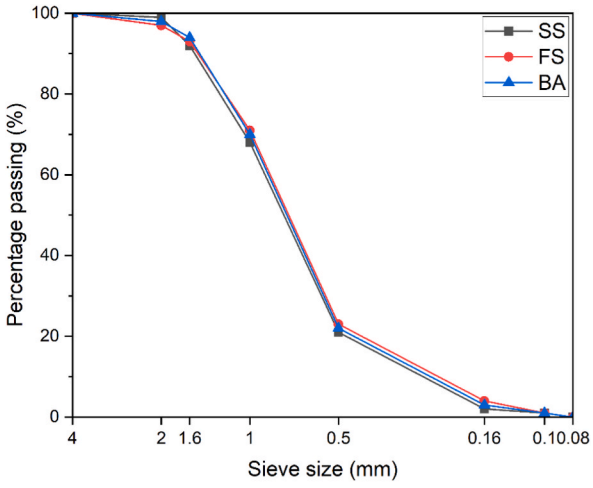

Fig. 1. Particle size distribution of aggregates.

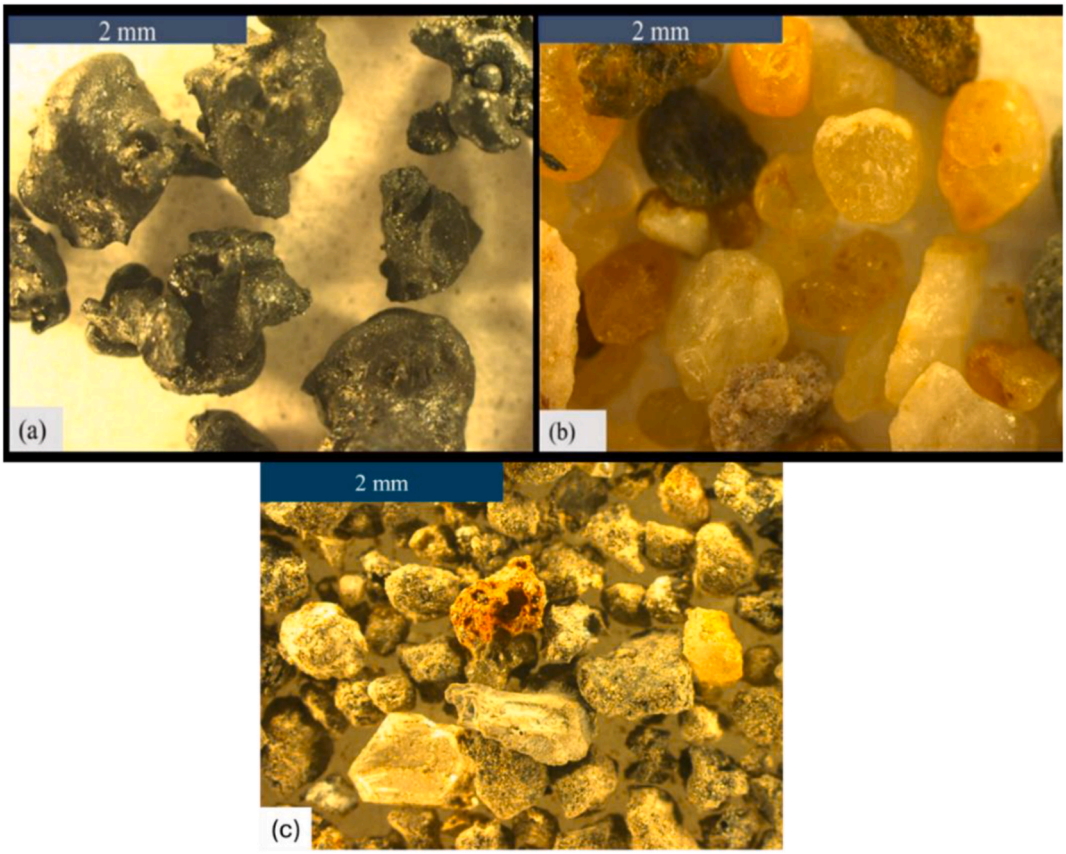

Fig. 2. Optical images of (a) FS, (b) SS, and (c) BA aggregates.

Table 1
Chemical composition, particle size distribution, LOI, and PLC density.

	PLC
SiO_2	15.2
Al_2O_3	3.5
Fe_2O_3	3.3
CaO	59.9
MgO	2.3
Na_2O	0.7
K_2O	0.8
TiO_2	0.2
P_2O_5	0.1
MnO	0.1
SO_3	5.0
Others	0.8
LOI at 950 °C	3.4
Density (g/cm^3)	3.1
d_{50} (μm)	9.2

2.2. Preparation of samples and curing conditions

Five mix proportions were developed for this study to assess the effect of replacing SS partly or wholly with either FS or BA on the fresh, hardened and durability properties of the mortar (Table 2). PLC was used as the cement for all the mixes. The aggregate-to-cement ratio for all the mixes was kept constant at 3:1, and the water-to-cement (w/c) ratio was fixed at 0.50 in accordance with the EN 196-1 standard [36]. The first mix, denoted by "SSM," is the reference mix containing SS, whereas those prepared by completely replacing SS with either FS or BA are denoted by FSM and BAM, respectively. The remaining two mixes (SSFSM and SSBAM) were prepared by replacing 50% of the SS aggregates with either FS or BA aggregates. All mortar samples were mixed through a mechanical

Table 2
Mix proportion of the mortar samples (kg/m^3).

	PLC	SS	FS	BA	w/c ratio
SSM	450	1350			0.5
FSM	450		1973		0.5
BAM	450			1454	0.5
SSFSM	450	675	987		0.5
SSBAM	450	675		727	0.5

process according to the EN 196–1 standard [36]. After the mixing operation, the fresh mortar samples were tested for their workability before casting them into oiled steel molds of dimension 50 mm × 50 mm × 50 mm^3 and 40 mm × 40 mm × 160 mm^3, which were compacted to remove air pockets using a jolting machine (60 shocks, 1/s). After compaction, the samples were placed in a plastic bag, properly wrapped, sealed, and cured at ambient temperature for 24 h. The mortar samples were carefully removed from the molds and placed in a humidity chamber at 23 °C and 90% relative humidity until the specified testing dates.

2.3. Test methods

2.3.1. Workability

The workability of the fresh mortar samples was assessed based on the spread diameter after applying 15 shocks using a flow table test in accordance with the EN 1015-3 standard [41]. The average of four spread diameter values was taken as the workability value.

2.3.2. Compressive strength

To assess the effect of different aggregate replacements on the mortar's mechanical properties, the compressive strength of all the mortar samples was measured in accordance with the EN-196-1 standard [36] using a calibrated Zwick Z100 testing machine (Zwick/Roell, Germany) with a maximum load of 100 kN and a loading force of 2.4 kN/s. Four cube samples for each mix at the specified curing age (3, 7, and 28 days) were tested, and the average compressive strength value was calculated. The standard deviation between the measured values was indicated by the strength measurement error bars. The compressive strength was calculated using the following equation:

$$\sigma = P/A$$

where σ is the compressive strength in N/mm^2, P is the load or force in N, and A is the cross-sectional area in mm^2.

2.3.3. Ultrasonic pulse velocity

The UPV of the mortar samples was measured to investigate the effect of different aggregates on the mortar's microstructural quality and compactness. The UPV test was performed according to the ASTM C597 standard [42]. Two 55-kHz transducers with a travel time accuracy of ±1% and a distance accuracy of ±2% were fitted to a UPV testing machine (Matest C369 N, Italy) with a measuring range of 0–3000 μs and an accuracy of ±0.1 μs. At each specified curing age (3, 7, and 28 days), triplicate prism samples for each mix were removed from the humidity chamber, and the UPV was measured. The UPV was calculated using the following equation:

$$V = L/T$$

where V is the UPV in m/s, L is the distance between the two transducers in m, and T is the transmission time in s.

2.3.4. Capillary water absorption

Four cube mortar samples (28-day age) of each mix were dried in a vacuum oven at 40 °C until a change in mass was less than 0.1%. The reason for drying at a lower temperature of 40 °C instead of 60 °C is to avoid ettringite decomposition, since ettringite decomposition usually starts around 60 °C. Capillary water absorption was performed in accordance with the ASTM C1585 standard [43]. After drying, the samples' surfaces were coated with epoxy, except for one surface, which was exposed and placed on the support rod in water. The mass of the samples was measured at different intervals for up to 8 days. The capillary water absorption was calculated using the following equation:

$$\textit{Capillary water absorption} = \frac{\Delta_m}{A}$$

where Δm is the change in the mass of the sample at time t (kg), and A is the exposure area of the sample in m^2.

2.3.5. Frost resistance

The frost resistance test was performed by exposing all the mortar samples to rapid freezing and thawing cycles in accordance with the ASTM C666/C666M − 15 standard [44]. Duplicate cube mortar samples (28-day old) were tested for each mix. Mortar samples were carefully placed in plastic containers in a climatic test chamber (WK3-180/40; Weiss Technik, USA). Water was added to the

containers containing the samples so that half (≈20 mm) of the samples were immersed in water and half were exposed to air. The water level was maintained throughout the frost resistance testing period. The samples were exposed to a total of 100 freeze-thaw cycles at a chamber temperature ranging from −18 to +4 °C. Each cycle took approximately 8 h and consisted of a 2 h dwell time at +4 °C, 2 h to decrease the chamber temperature to −18 °C, 2 h dwell time at −18 °C, and 2 h to increase the chamber temperature to +4 °C. Visual observation, mass loss, and residual compressive strength of all mortars were measured after exposure to freeze-thaw in water.

2.3.6. Combined resistance to sulfate and chloride

Duplicate cube mortar samples (28-day age) for each mix were exposed to freeze-thaw cycles in combined sulfate and chloride solutions to simulate marine conditions in temperate/cold regions and exposure to saline conditions during winter. A mixture of 5% sodium sulfate (product code 1.06649.0500 by Merck, Germany) and 3% sodium chloride (product code 7647-14-5 by J. T. Baker, the Netherlands) was used to prepare the solution as suggested in Ref. [5]. The solution level and pH were checked at 25, 50, 75, and 100 cycles to ensure they were kept constant throughout the testing period. The effect of mortar exposure to combined sulfate and chloride solutions was assessed in terms of mass loss, visual appearance, and residual compressive strength.

2.3.7. Alkali–silica reaction

The ASR of the aggregate systems was assessed according to the ASTM C1260 standard [45]. Five aggregate systems were examined to produce the mortar bars for the test. The reference mortar was produced using SS as the aggregate (named "SS"). Two other mortar mixes containing FS (named "FS") or BA (named "BA") as aggregates were prepared to assess the effect of full replacement of SS with either FS or BA on ASR. The remaining two mortar mixes were binary blends (SS + FS and SS + BA) produced by partially replacing SS with either FS or BA. CEM II 42.5 N PLC was used as the binder in all mixtures.

After casting, the mortar bars were demolded after 24 h and stored in water at 80 °C for an additional 24 h. The initial comparator readings were obtained immediately before immersion in 1 M NaOH solution at 80 °C, marking the beginning of the accelerated ASR exposure. Measurements were recorded after 7, 14, 21, and 28 days of immersion in NaOH. Expansion was calculated relative to the initial reading, and the replicates' mean and standard deviation were reported. The results were interpreted based on the ASTM C1260 criteria, where expansions exceeding 0.10% at 14 days indicate potential reactivity, and values above 0.20% denote highly reactive aggregate behavior. The expansion measurements were performed using a length comparator. The expansion of the mortar bars was calculated as the percentage change in length relative to the initial reference length. Here, L_0 is the initial length, and L_t is the length measured at the specified test age. The expansion was calculated using the following equation:

$$Expansion\ (\%) = \frac{L_t - L_0}{L_0} x100$$

2.3.8. X-ray diffraction

XRD analysis of the precursors and mortar samples was performed using a Rigaku SmartLab 9-kW diffractometer (Japan). The measurement was made using CoKα radiation at 40 kV, a current of 135 mA, a scanning speed of 4° 2θ/min, and a step size of 0.02° over a scanning range of 2θ = 5–130°. The Rigaku PDXL 2 software with the PDF-4+ 2020 RDB database was used for phase identification and quantification.

2.3.9. SEM-EDS

SEM micrographs of the prepared mortar samples were obtained using SEM-EDS analysis (Zeiss Ultra Plus, Germany). Secondary and backscattered electron images were captured at an acceleration voltage of 15 kV and a working distance of 8 mm. Before obtaining

Table 3
Leaching test results of FS and BA aggregates performed in accordance with EN12457-2 and limits specified by Finnish legislation (843/2017).

Hazardous elements	Element concentration (mg/kg)			
	Covered structure	Paved structure	FS	BA
pH	**N/A**	**N/A**	**9.59**	**11.48**
Conductivity (mS/cm)	**N/A**	**N/A**	**0.05**	**0.73**
As	0.5	1.5	0.005	0.14
Ba	20	60	0.036	3.1
Cd	0.04	0.06	<0.001	<0.002
Cr	0.5	5	0.009	0.45
Cu	2	10	0.05	<2
Hg	0.01	0.03	<0.002	<0.004
Mo	0.5	6	0.007	0.3
Ni	0.4	1.2	0.14	<0.01
Pb	0.5	2	0.003	0.015
Se	0.4	1	0.021	<0.04
Zn	4	12	0.032	0.8
Cl	800	2400	25	25
F	10	50	<5	<5

the SEM micrographs, the samples were carefully cut into small pieces, cast in epoxy resin, polished using ethanol, and carbon coated.

3. Results and discussion

3.1. Environmental aggregate leaching

Table 3 presents the leaching test results of alternative fine aggregates used for mortar production. All elements released from the aggregates were below the allowable regulatory limits specified by Finnish government legislation on the recovery of certain wastes for use as aggregates in earth construction (paved and covered structures) [46]. Based on the leaching results, the aggregates can be regarded as eco-friendly materials that can be used as alternative secondary aggregate materials in the construction industry. The use of FS and BA as alternative aggregates in cement mortar production complies with the European Union's zero waste, circular economy, and sustainability principles [47].

3.2. Microstructural characterization

3.2.1. SEM

The SEM micrographs of representative sections of mortar samples (500× and 2000× magnifications) after 28 days of curing are presented in Fig. 3a–j. Microcracks were present in the gel of all samples, and this became more pronounced at higher magnifications. The presence of microcracks during SEM analysis may be attributed to specimen preparation or exposure to vacuum conditions. Meanwhile, differences in the interfacial transition zone (ITZ) and bonding ability were observed among the samples. For instance, the reference sample containing SS (SSM) exhibited a homogeneous microstructure and dense ITZ, which was more evident at higher magnifications. No visible bond cracks were observed at the aggregate-matrix interface, indicating higher microstructural compactness and enhanced SS–matrix cohesion. Moreover, the FSM mortar samples showed a microstructure comparable to that of SSM. Similar to SSM, the microstructure of FSM appeared dense with no bond crack propagation at the aggregate-matrix interface, indicating higher affinity and bonding between the FS and the matrix. Conversely, BAM showed a less homogeneous and loose microstructure, which was characterized by the presence of pores in the aggregate and gel, which were not filled with hydration products. This may have contributed to the weak ITZ observed between the BA and the matrix. Furthermore, SSBAM displayed a heterogeneous microstructure with pores. A strong interface was observed near the SS aggregate, whereas a weak interface was observed near the BA aggregate. The difference in the mortar ITZ properties may be attributed to the difference in the properties of BA and SS. For instance, the high sorptivity and porous nature of BA compared to SS may have contributed to its weak ITZ in the mortar. Meanwhile, SSFSM exhibited a homogeneous microstructure and a denser ITZ, which was attributed to the efficient packing and higher affinity among the mortar components. The FS and SS were properly distributed and integrated in the matrix, and no bond cracks were found at the interface, indicating strong bonding and increased microstructural compactness. Based on the SEM results, the difference in the microstructure is expected to significantly influence the physical, mechanical, and durability properties of the mortar samples (as discussed in the subsequent sections).

3.3. Fresh properties

3.3.1. Workability

Fig. 4 shows the workability of all fresh mortar mixes. The results showed that the aggregate type influences the workability of all mixes. Partial or total replacement of SS with either FS or BA significantly reduced mortar workability. Of all the mixes, the reference mortar (SSM) containing SS aggregates exhibited the highest workability, whereas the BAM mortars containing BA aggregates exhibited the lowest workability. The highest workability of SSM may be attributed to the round shape, smooth surface, and low water absorption characteristics of SS (see Section 2.1). Owing to the low water absorption of SS, more free water was available to lubricate the matrix during mixing, resulting in enhanced workability. In addition, the round shape and smoother surface of SS helped reduce shear resistance in the mortar mix, resulting in improved workability. Alternatively, the total replacement of SS with BA reduced the workability values of BAM by 34% compared to the reference mix (SSM). This reduction in the workability of BAM may be attributed to the irregular shape, rough surface, porous nature, and higher water absorption characteristics of BA (see Section 2.1). The porous nature and high water absorption characteristics of BA mean that more water was needed for the mortar's wettability due to a reduction in the amount of free water available for lubrication. These BA characteristics are presumed to have caused increased internal friction in the mortar matrix, resulting in less fluidity and workability. The results of this study are consistent with those reported in the literature [30,48,49].

Furthermore, the total replacement of SS with FS resulted in lower workability of FSM compared to SSM at a similar volume ratio, which was attributed to the angular shape of FS, which increases the frictional resistance among the mortar components, resulting in lower workability. This is consistent with some reported studies where a decrease in workability was observed when sand was replaced by copper slag, mainly attributed to its angular shape [50,51]. However, FSM exhibited higher workability than BAM. Unlike BAM, whose workability was reduced by 34%, the workability of FSM was reduced by 11% compared with that of SSM. The higher workability of FSM compared to BAM may be attributed to the low water absorption characteristics and non-porous nature of the FS aggregate (see Section 2.1). This means that less water was absorbed by FS than by BA, making more water available as a lubricant between solid particles, thereby reducing the interparticle frictional force and enhancing workability. Meanwhile, partial replacement (50%) of SS with FS enhanced the workability of SSFSM mortars compared with those made with 100% FS (FSM). Similarly, partial

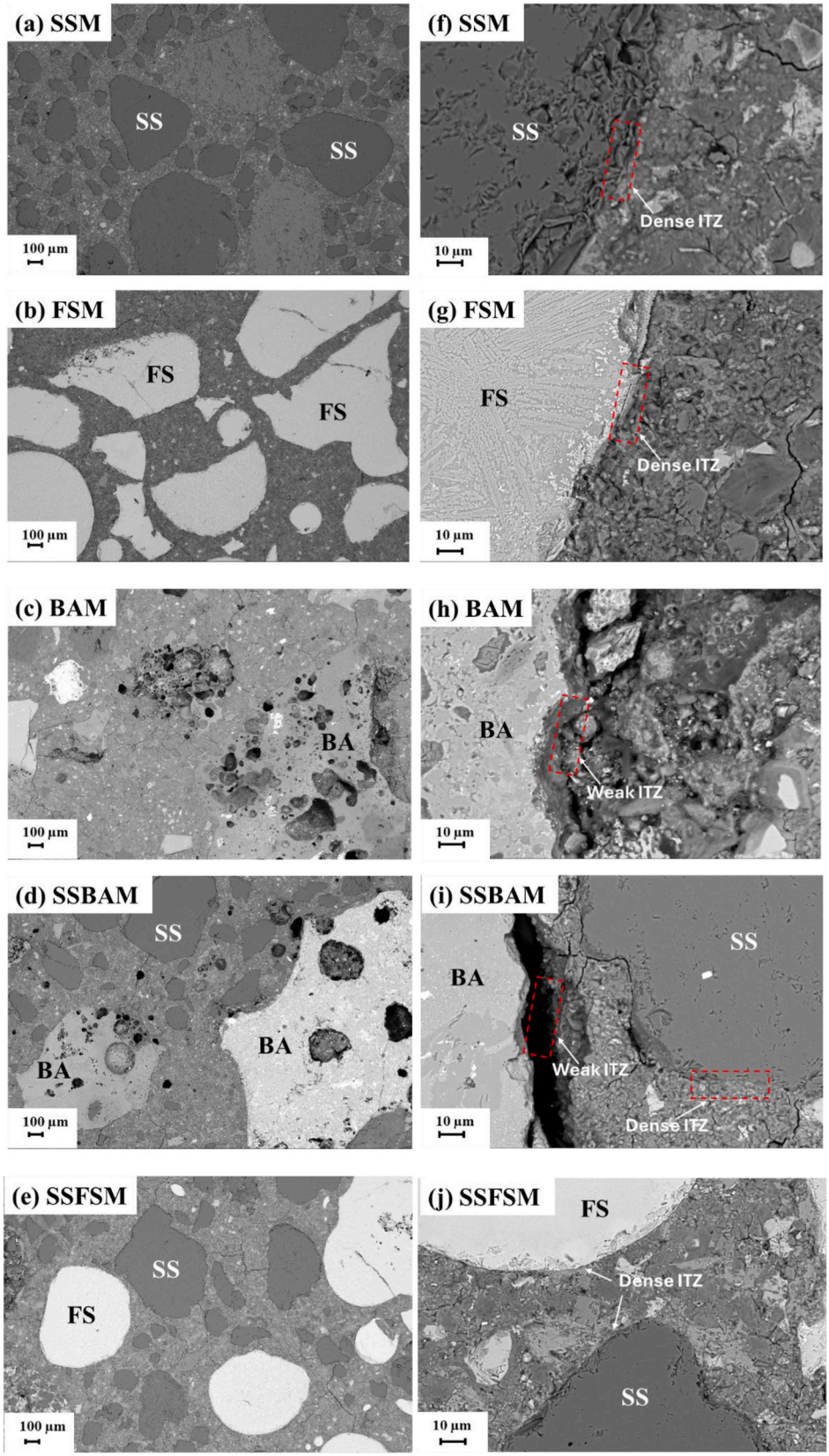

Fig. 3. SEM micrographs of the mortar samples after curing for 28 days.

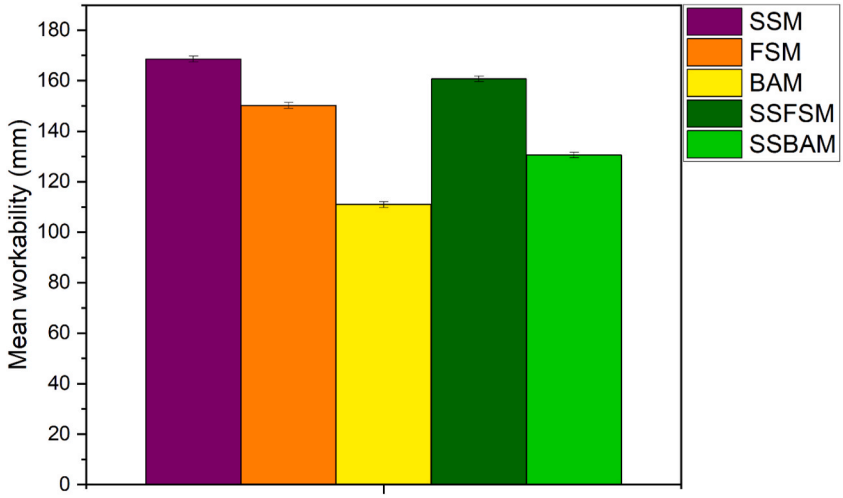

Fig. 4. Workability of the mixes.

replacement of SS with BA enhanced the workability of SSBAM compared with that of 100% BA (BAM). Hence, the partial replacement of FS or BA with SS is beneficial for the workability of SSFSM and SSBAM mortars. Meanwhile, some mixes, particularly those containing BA aggregates, exhibited extremely low workability compared to the reference mix. Thus, using a superplasticizer or other workability-enhancing admixtures is recommended to achieve comparable workability values to the reference mix. From the results, it can be inferred that the aggregate properties play a critical role in influencing the workability of the mortar mixes.

3.4. Properties of hardened mortar

3.4.1. Compressive strength

The compressive strengths of all the mortar samples are presented in Fig. 5. The compressive strength of all samples increased with curing age, regardless of the aggregate type, indicating that the samples underwent continuous hydration and strength development

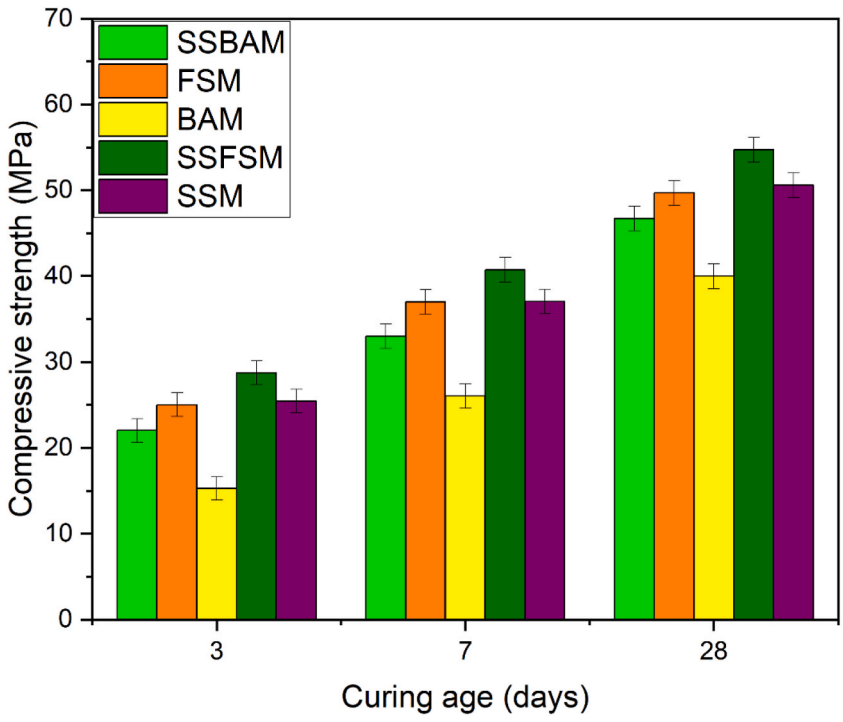

Fig. 5. The compressive strength of the mortar samples.

over time. At an early age, the compressive strength of all samples ranged from 15 to 29 MPa, with BAM having the lowest compressive strength and SSFSM having the highest compressive strength. The full replacement of SS with BA resulted in lower early-age compressive strength compared with the reference mix (SSM). However, full replacement of SS with FS resulted in comparable early-age strength when compared to SSM, with SSM and FSM showing an early-age compressive strength of 25 MPa. Meanwhile, the partial replacement of SS with either FS or BA resulted in higher early-age compressive strength compared with the corresponding mortars containing 100% FS or BA (FSM and BAM). SSFSM mortars containing a mix of SS and FS exhibited a compressive strength of 29 MPa, whereas FSM mortars containing 100% FS exhibited a compressive strength of 25 MPa. In addition, SSBAM containing a mixture of SS and BA exhibited a compressive strength of 22 MPa, whereas BAM containing 100% BA aggregates exhibited a compressive strength of 15 MPa.

A similar trend was observed for the 7- and 28-day compressive strength, with mortar samples containing a mix of SS and FS aggregates achieving the highest 28-day compressive strength of 55 MPa. The lower compressive strength exhibited by BAM compared to SSM and FSM at all ages could be attributed to the aggregates' physical and chemical properties. The porous nature, low hardness, and inferior mechanical properties of BA aggregates are believed to have adversely influenced the compressive strength of BAM. The high water absorption of BA may have caused incomplete cement hydration, resulting in lower strength. In addition, the weak bonding between BA and cement observed in the SEM analysis (see Section 3.2.1) may have contributed to the lower compressive strength of BAM than that of other samples. The lower compressive strength observed in the mortar samples containing 100% BA aggregates in this study is consistent with those reported in the literature [52,53]. Although FS and BA have similar angular shapes, FSM had higher compressive strength than BAM at a similar replacement ratio. This may be attributed to the dense and non-porous nature of FS and the strong bonding between FS and cement (see Section 3.2.1), leading to a denser microstructure and better strength development. In addition, SSM and FSM exhibited comparable mechanical properties at all ages, indicating that the full replacement of SS with FS does not have any adverse effect on the mechanical properties. Similar observations have been reported in our previous study [54]. Meanwhile, the partial replacement of SS with FS resulted in complementary advantages and improved compressive strength compared with the reference mix (SSM) and those containing 100% FS aggregates (FSM). One possible explanation could be that the mixture of FS and SS with different properties is believed to have provided a dual effect of bonding and pore filling ability, resulting in better particle packing, enhanced pore refinement, and higher compressive strength of SSFSM. This result is consistent with those observed and reported in the literature [11,55]. The optimal compressive strength was achieved when 50% of the sand was replaced by copper slag, with the compressive strength surpassing that of the reference mix [11,55]. Moreover, partial replacement of SS with BA resulted in higher compressive strength compared with those containing 100% BA aggregates.

However, the compressive strength of the BA aggregate-containing mortars (BAM and SSBAM) was lower than that of the reference samples (SSM) at all ages. This indicates that partial or full replacement of SS with BA has a negative effect on mortar strength. This result is consistent with those reported in the literature, where a reduction in compressive strength was observed when more than 25% of the sand was replaced by BA [7,30,31,49]. The reduction in compressive strength was attributed to the higher porosity and water absorption of BA, the presence of microcracks, and the lower structural compactness of BA-containing mortars [7,30,31,49]. Overall,

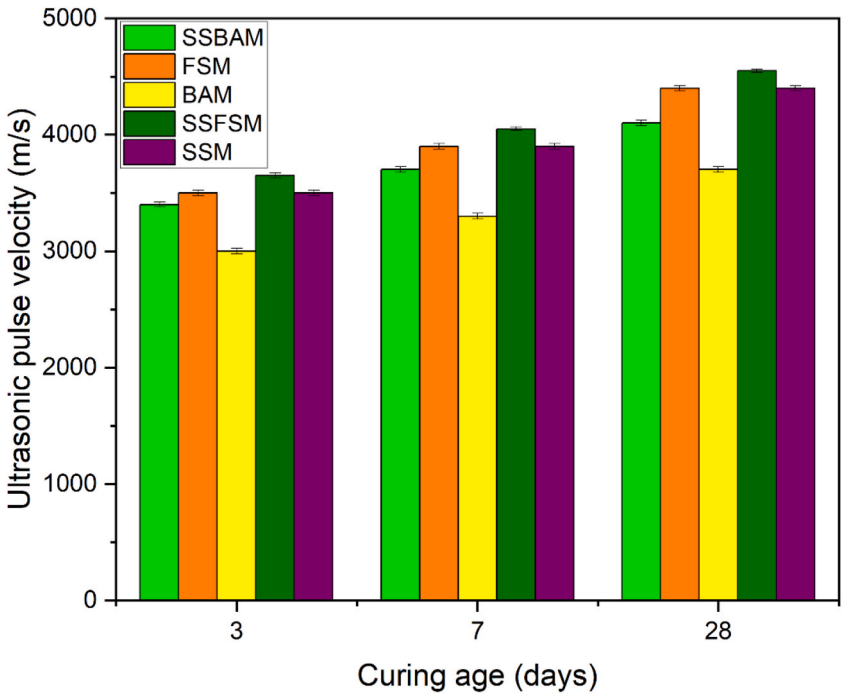

Fig. 6. The ultrasonic pulse velocity of the mortar samples.

after 28 days, the strength achieved in all the mortar samples meets the compressive strength requirements for light traffic paving brick, structural clay load-bearing wall tile, and building brick [56].

3.4.2. Ultrasonic pulse velocity

The UPV is a non-destructive test that can be used to measure mortar quality and microstructural development over time and can be a valuable indicator of mortar porosity [9]. The UPV value of all mortars increased with increasing curing age, indicating continuous hydration and microstructural development over time (Fig. 6). However, the UPV values varied among the samples and were mainly influenced by the aggregate type. The SSFSM mortar samples had the highest UPV value, whereas the BAM samples had the lowest UPV value at all ages. For samples containing 100% BA aggregates, the UPV value was lower than that of the reference samples containing 100% SS aggregates and samples containing 100% FS aggregates. This is because the physical and chemical properties of BA and FS differ from those of SS. For instance, if the mortar pores were not filled with cement paste, the use of porous BA as aggregate can increase its porosity, which may be one of the primary reasons why BAM had the lowest compressive strength and higher capillary water absorption (see Sections 3.4.1 and 3.5.2). Porosity is one of the main factors influencing the UPV value [4]. The higher the porosity, the lower the UPV value. In addition, the lower chemical bonding between BA and cement, weak ITZ, and the presence of pores affected the microstructural compactness (see Section 3.2.1), resulting in a lower UPV value of BAM. Thus, the higher UPV values of FSM and SSM compared to BAM could be attributed to their lower porosity and enhanced cohesion at the ITZ between the cement and aggregate surface. This result is consistent with those reported in the literature, where the mortar or concrete's quality and microstructure depended on the interlocking force and cohesion between the cement paste and aggregate [4,57].

Furthermore, SSM and FSM had similar UPV values, suggesting that both samples had comparable mortar quality and compactness. Meanwhile, partial replacement of SS with BA resulted in a higher UPV value of SSBAM mortars compared to BAM mortars. Similarly, the partial replacement of SS with FS had a remarkable positive effect on the UPV values of the SSFSM. This is because the use of a mix of aggregates with different characteristics (e.g., shape, density, and water absorption) is believed to have enhanced the packing of particles, reduced the mortar's porosity and voids, and increased the mortar components' affinity, which is crucial for the mortar's quality and microstructure. This may be one of the primary reasons why the UPV values of SSFSM and SSBAM were higher than those of their corresponding FSM and BAM. The highest UPV values measured in the SSFSM indicated that the matrix had fewer voids and defects and was denser and more compact than the remaining samples, provided that all samples had comparable stiffness. The UPV values of all mortars are consistent with the SEM analysis and compressive strength measurements (see Section 3.2.1 and 3.4.1). Based on the Leslie and Cheeseman [58] classification of mortar and concrete quality, the UPV value of mortar can be classified as excellent (>4570 m/s), good (3660–4570 m/s), doubtful/questionable (3050–3660 m/s), poor (2130–3050 m/s), and very poor (<2130 m/s). In accordance with the mortar/concrete quality criteria, the UPV values of all the mortar samples after 28 days were in the range of 3700–4550 m/s and can therefore be classified as good mixes.

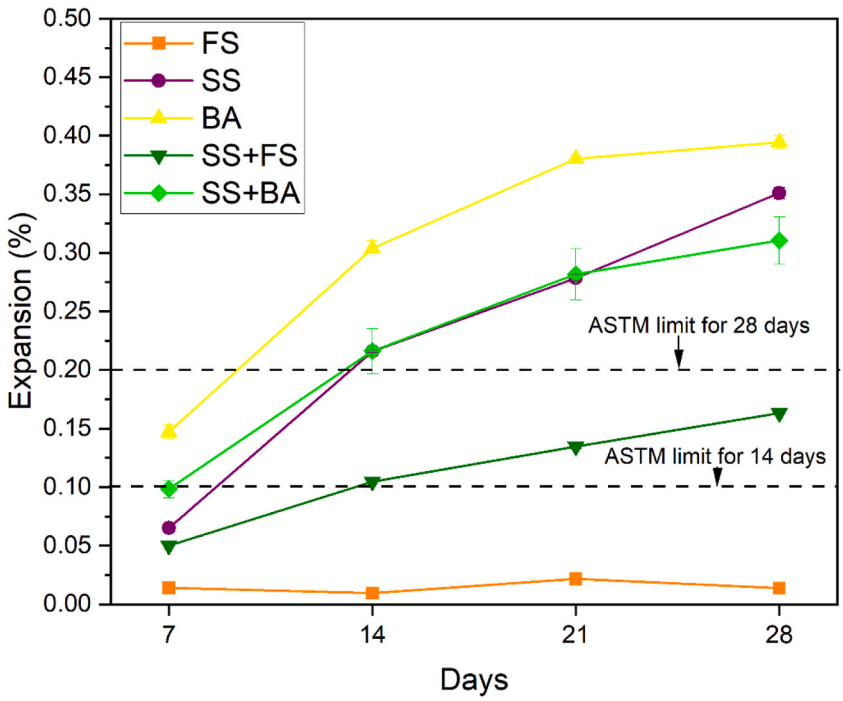

Fig. 7. The accelerated mortar bar expansion of the FS, SS, BA, SS + FS, and SS + BA mixtures was measured in accordance with ASTM C1260.

3.5. Durability properties

3.5.1. Alkali–silica reaction

All aggregates exhibited distinct ASR responses and expansion rates (Fig. 7). FS exhibited the lowest expansion rate among all tested materials, with 14- and 28-day expansion rates of 0.009% and 0.014%, respectively, indicating nonreactive behavior under accelerated conditions. Conversely, SS had a higher expansion rate than FS, reaching 0.216% and 0.351% after 14 and 28 days, respectively, indicating that SS is moderately reactive. BA had the highest expansion rate of 0.304% in 14 days, which increased to 0.394% after 28 days. Therefore, BA can be classified as a highly reactive aggregate. Meanwhile, the use of binary aggregates demonstrated intermediate behavior compared with their respective individual aggregates. For instance, the SS + FS blend exhibited reduced expansion rates compared with pure SS at 14 and 28 days, indicating that the partial replacement of SS with FS provides a mitigation effect, resulting in lower expansion rates. Similarly, the SS + BA blend exhibited lower expansion than pure BA at 14 and 28 days. This indicates that the dilution of BA with SS decreases the overall expansion. However, the expansion rate of SS + BA and BA was >0.2% after 14 and 28 days, indicating that both systems can be classified as reactive. The standard deviations were generally low across all mixtures and test ages, demonstrating strong repeatability and reliability of the measurements. According to ASTM C1260 specifications limits for ASR, the expansion rate for aggregates at 14 days should be below 0.1%, whereas the expansion rate of aggregates at 28 days should be below 0.2%. With reference to the ASTM limit for 14 days, SS, SS + FS, BA, and SS + BA exceeded the limit, and only FS met the requirement. However, SS, BA, and SS + BA exceeded the ASTM limit for 28 days, and only FS and SS + FS

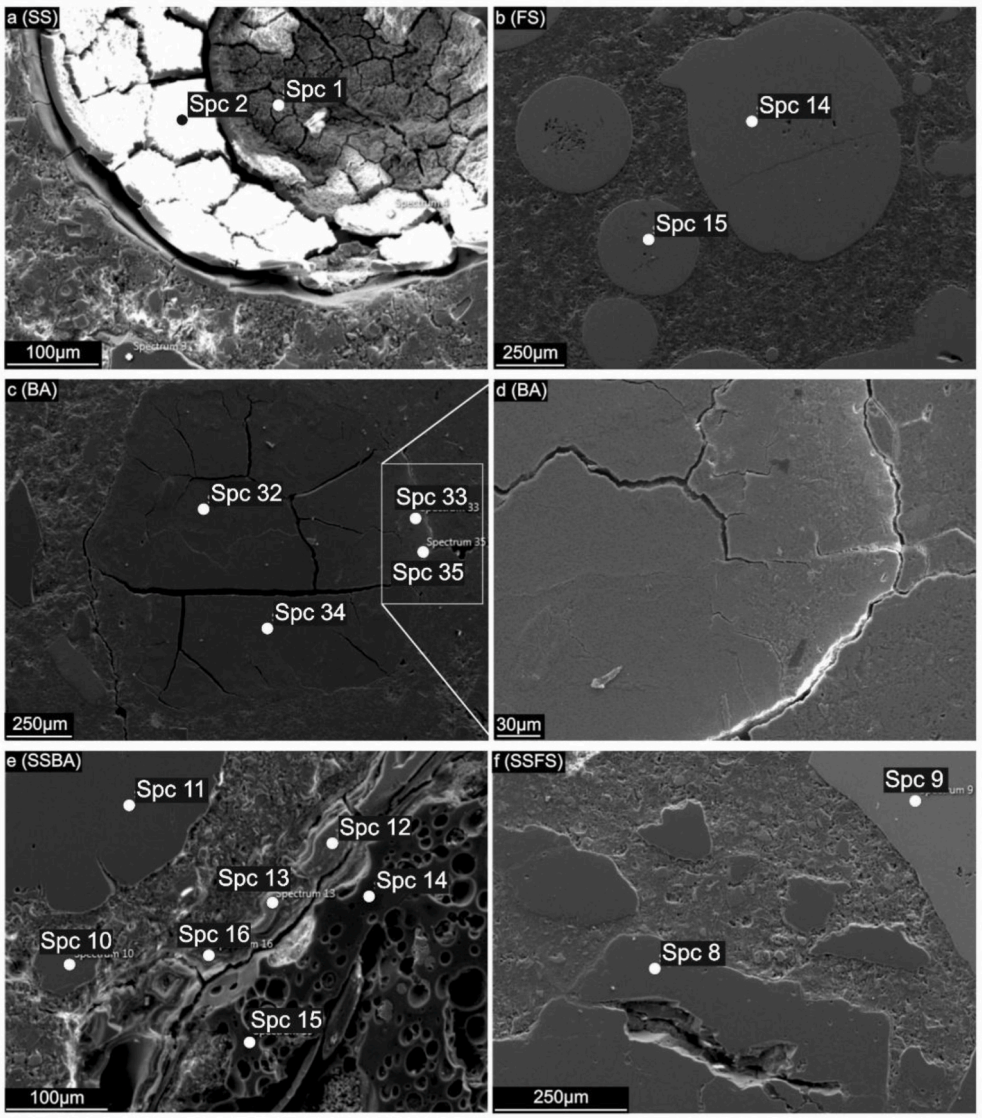

Fig. 8. SEM micrographs and corresponding EDS measurement points for all mortar systems (spc: spectrum).

met the requirement.

SEM imaging of SS showed widespread reaction products within and around the siliceous grain, characterized by cracked and porous ASR gel morphology (Fig. 8a). EDS analyses (Spectra 1–4) revealed Na–Si-rich and Ca-poor compositions (Si = 17–24 wt%, Na = 7–9 wt.%), consistent with alkali–silicate hydrate gels identified in recent mechanistic studies [59]. The observed degradation features are explained by the alkaline dissolution of siliceous phases and subsequent precipitation of Na/K-bearing gels, as reported experimentally by Ref. [60]. The intragranular cracking and gel-filled regions suggest that the reactive phase, likely quartz mixed with siliceous microcrystalline components such as chert, underwent significant alkaline alteration. Similar internal gel accumulation and cracking patterns have been documented in highly reactive silica systems [61–63]. Overall, the observed chemistry and morphology confirm the presence of advanced ASR in the reference SS mortar. This microstructural evidence is consistent with the high expansion values measured for SS in the accelerated mortar bar test (Fig. 7), indicating that the observed deterioration is directly associated with the formation of the classical ASR gel.

In the FS sample, the SEM observations showed large, dense, and smooth-edged Fe-rich grains (Fig. 8b). EDS analyses (Spectra 14–15) confirmed a dominant Fe–Si composition (Fe ≈ 42 wt%, Si ≈ 17–18 wt%) with negligible alkalis and Ca, indicating that this phase is inert under alkaline conditions. No visible Na–Si-rich ASR gel, dissolution features, or reaction rims were observed. The internal cracks observed within the grain appeared to be inherent microstructural features rather than ASR-induced damage, confirming the nonreactive behavior of the FS aggregate. This result is consistent with the negligible expansion values measured for FS in the accelerated mortar bar test (Fig. 7), further supporting its inert behavior under alkaline conditions.

SEM-EDS analyses of the BA sample (Fig. 8c and d) revealed no morphologically or chemically distinct ASR gel on crack surfaces or around BA particles despite the relatively high expansions measured in accordance with ASTM C1260. Instead, SEM imaging showed characteristic whitening and surface softening at the edges of BA grains, indicating localized degradation of the glass phase rather than classical gel formation. This finding is consistent with previous findings showing that ASR-related products in BA-containing systems do not necessarily manifest as Na–K–Si-rich, low-Ca gels associated with reactive siliceous aggregates. Müller and Rübner [64] reported that ASR products in BA-containing concretes frequently remain confined within internal pores without forming visible gel rims. Similarly, Schafer et al. [65] noted that the amorphous glassy phases in BA undergo internal alkali-induced degradation, producing reaction products that accumulate within the particle interior rather than extruding into cracks. Consistent with this behavior, EDS measurements from crack margins (Spectra 32–35) showed elevated Ca contents (≈30–34 wt%) and relatively low Si concentrations (9–15 wt%), which correlate well with the pale, chalky appearance observed along particle edges (Fig. 7d). These high Ca/Si ratios (~2–3) point to Ca-rich hydrate precipitates rather than ASR gel. Comparable Ca-enriched surface phases have been documented by Abbas et al. [66]. Variations in Na (1–4 wt.%), Al (2–10 wt%), and Mg further reflect the BA's heterogeneous, partly devitrified structure. Altogether, these features indicate that the whitening and cracking observed around BA particles arise from surface hydration and alkali-induced alteration of the glassy phase, rather than ASR gel formation, explaining the absence of visible ASR gel despite the measured expansions. This suggests that the expansion measured in BA mortars is not directly associated with the formation of the classical ASR gel but with the internal degradation and volumetric instability of the amorphous glassy phase.

SEM-EDS analyses confirmed the coexistence of SS-derived and BA-derived phases in the SS + BA sample. Spectrum 11 exhibited a Si-rich composition (Si ≈ 51 wt%), which corresponds to a natural sand grain. Minor whitening and fine reaction traces around this particle suggested the onset of limited ASR-related alteration, although gel development remained minimal (Fig. 8e). Conversely, Spectra 10, 12, 13, 15, and 16 were characterized by Ca-rich compositions (27–53 wt% Ca), representative of BA particles. These regions exhibited clear edge whitening, surface degradation, and inward-progressing Ca enrichment (Fig. 8e). The larger BA particle analyzed showed peripheral whitening and brittle fracture features. These observations indicate two parallel behaviors: a very minor degree of ASR-related alteration at isolated sand grains and a more dominant cracking response governed by BA particles. Thus, in the SS + BA mixture, cracking is primarily driven by BA-related microstructural weakness, whereas SS-derived ASR gel formation remains limited and scattered. This combined behavior is consistent with the measured expansion trend, where the initial dilution of reactive silica reduces early expansion, whereas the progressive degradation of BA contributes to increased expansion at later ages.

SEM-EDS analyses of the SS + FS sample revealed the combined effects of reactive sand (SS) and the Fe-rich, nonreactive silicate aggregate (FS). Spectrum 8 corresponded to a Si-rich sand grain exhibiting a few internal microcracks; however, these crack interiors were completely empty, indicating that ASR did not progress within the particle (Fig. 8f). Spectrum 9 displayed a strongly Fe-dominated composition typical of the FS phase and showed no dissolution features or reaction rims. Although the SS component possesses inherent ASR potential, the presence of FS significantly limited the reaction development. The FS phase does not consume or chemically bind NaOH; however, its inert nature reduces the amount of available reactive silica and restricts ionic mobility within the mortar. Consequently, the overall system becomes less conducive to ASR initiation, preventing sand grains from reaching the required activation threshold for gel formation. This behavior is reflected in the SS + FS mortar expansions, which remained well below the ASTM limit and corresponded to the absence of gel in both aggregate types. This further confirms that the reduced expansion is directly associated with reactive silica dilution and ASR development suppression in the system.

Overall, the expansion behavior is strongly dependent on the mineralogical nature of the aggregates and the associated reaction mechanisms. While the expansion in siliceous aggregates, such as SS, is governed by classical ASR gel formation, alternative mechanisms, such as glassy phase degradation in BA and dilution effects in blended systems, also play a significant role in controlling expansion.

3.5.2. Capillary water absorption

The rate of penetration and transportation of water, including various destructive acids and salts, from the surroundings into the mortar is usually investigated by capillary water absorption. The easier the penetration and transportation of water, the higher the

absorption and deterioration rate of mortars after exposure. Fig. 9 shows the capillary water absorption of all mortar samples. The results showed that the capillary water absorption of the mortar samples increased over time until it became stable, regardless of the aggregate type. However, the water penetration and transportation rates into the samples differed. Out of all the mixes, SSFSM exhibited the lowest capillary water absorption, whereas BAM exhibited the highest capillary water absorption. Total replacement of SS with BA aggregates resulted in higher capillary water absorption of BAM mortars compared with the remaining mortars. The highest capillary water absorption observed in BAM may be ascribed to its higher levels of permeability and porosity, as indicated by its lower UPV measurements and compressive strength (see Section 3.4.1 and 3.4.2) and the presence of pores in SEM measurements (see Section 3.2.1). Huynh and Ngo [7] reported a direct correlation between porosity and other indices, such as water absorption, UPV, and compressive strength, of cement mortars containing BA as fine aggregates. Therefore, the higher capillary water absorption observed in BAM can be attributed to the porous nature of the incorporated BA aggregates, which increases the capillary pore connectivity levels and void content, thereby creating an easy water penetration pathway. This result is consistent with those reported in the literature, where the water absorption of masonry blocks containing 100% BA aggregates is almost three times higher than that of conventional masonry blocks containing sand as aggregates [67].

In contrast, FSM exhibited comparable capillary water absorption, but lower capillary water absorption compared to BAM, likely attributed to the higher bonding characteristics, low water absorption, and non-porous nature of FS compared to BA. Moreover, the partial replacement of SS with BA resulted in lower capillary water absorption of SSBAM than that of BAM. Similarly, partial replacement of SS with FS resulted in lower capillary water absorption of SSFSM than that of FSM. Meanwhile, the effect of partial replacement of SS with FS was more beneficial to the microstructure of SSFSM, resulting in the lowest capillary water absorption compared with the remaining mortar samples. This means that the use of a mix of FS and SS enhanced particle packing, reduced permeability and pore connectivity in the mortar matrix, resulting in lower capillary water absorption. Therefore, the lowest capillary water absorption observed in SSFSM may be attributed to its denser and more compact microstructure, consistent with its highest compressive strength and UPV values (see Sections 3.4.1 and 3.4.2).

3.5.3. *Freeze-thaw in water*

Freeze-thaw resistance of mortar samples is one of the most important durability properties, particularly if they are to be used as outdoor materials (e.g., paving blocks) in temperate/cold regions. The exposure of all the mortar samples to 100 freeze-thaw cycles in water was evaluated in terms of visual observation, mass loss, and residual compressive strength (Figs. 10–12). In terms of visual observation (Fig. 10), all the samples exhibited relatively high stability after exposure to freeze-thaw cycles in water. No significant macrocracks or visible damage were observed in any of the samples, indicating their potential to withstand severe frost conditions. Meanwhile, all the samples exhibited mass loss after exposure, with SSM, FSM, BAM, SSFSM, and SSBAM showing mass losses of approximately 0.60%, 0.63%, 1%, 0.50%, and 0.90%, respectively. In addition, all the samples exhibited a reduction in compressive strength after exposure, with SSM, FSM, BAM, SSFSM, and SSBAM samples exhibiting strength losses of approximately 17%, 18%, 38%, 10%, and 23 %, respectively. BAM exhibited the highest mass loss and strength reduction, whereas SSFSM exhibited the lowest

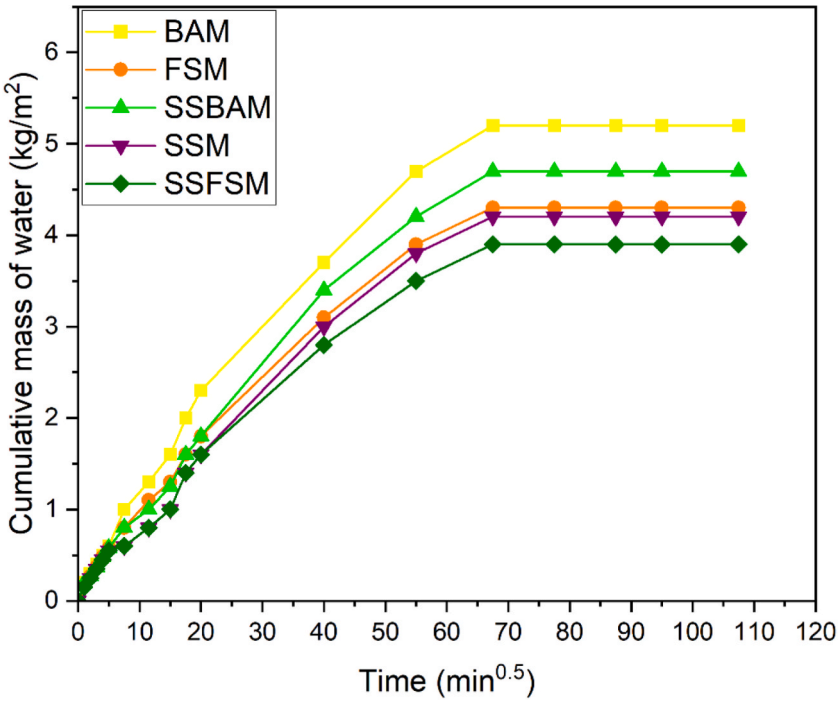

Fig. 9. Capillary water absorption of mortar samples after curing for 28 days.

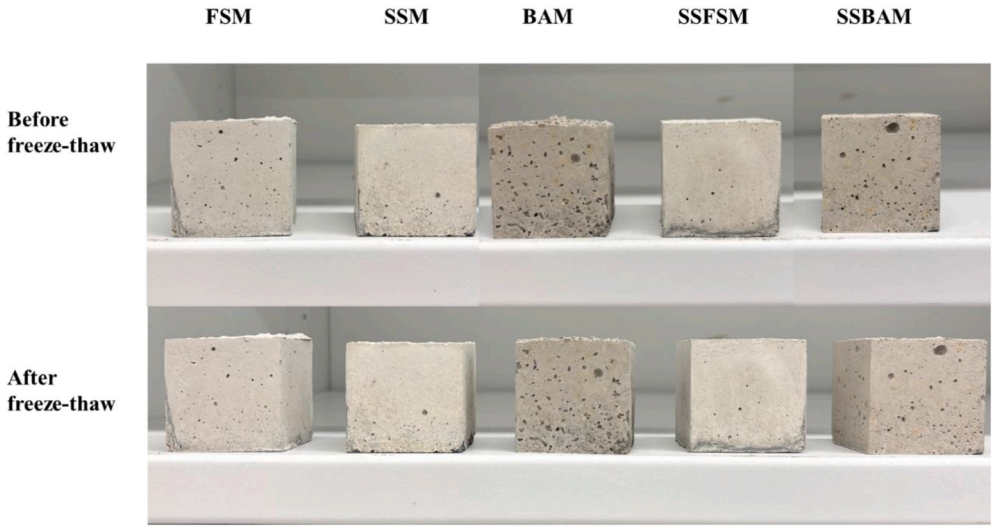

Fig. 10. Visual observation of the mortar samples before and after freeze-thaw exposure.

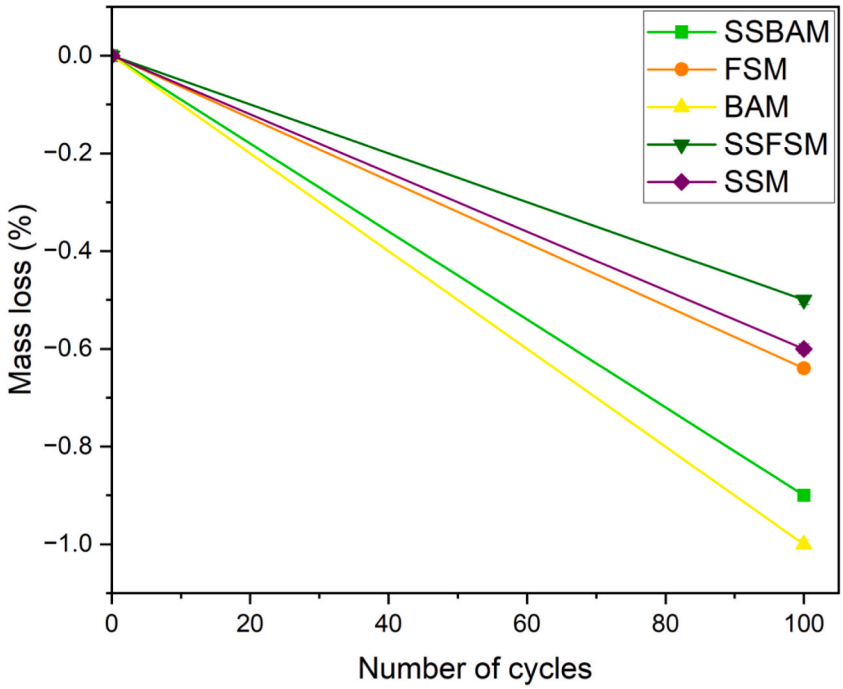

Fig. 11. Mass loss of mortars due to freeze-thaw exposure.

mass loss and compressive strength reduction. It is worth stating that the freeze-thaw resistance of materials is mainly governed by three factors: pore size distribution, porosity, and mechanical properties [24,68]. It has been recognized that better freeze-thaw resistance can be achieved if a certain share of pores is greater than 3 μm. In addition, the samples must have a high mechanical strength to withstand the force due to ice expansion. Finally, the sample must have a low porosity to resist the ingress of water into the structure. Therefore, the mass and strength loss of the samples after exposure to freeze-thaw conditions in water were mainly ascribed to the penetration and transportation rate as well as the volume expansion of the absorbed water in the pores. In addition, the infiltration and penetration of water molecules inside the pore cavities, coupled with the freeze-thaw action, can weaken the mortar microstructure, resulting in lower mechanical properties [5]. The rate of water infiltration and penetration is likely to increase with time, particularly in samples with higher porosity.

Therefore, the higher mass and strength loss in BAM can be attributed to its higher porosity and less compact microstructure, as indicated by its lower UPV, higher capillary water absorption measurements, and weak ITZ (see Sections 3.2.1, 3.4.2, and 3.5.2). This

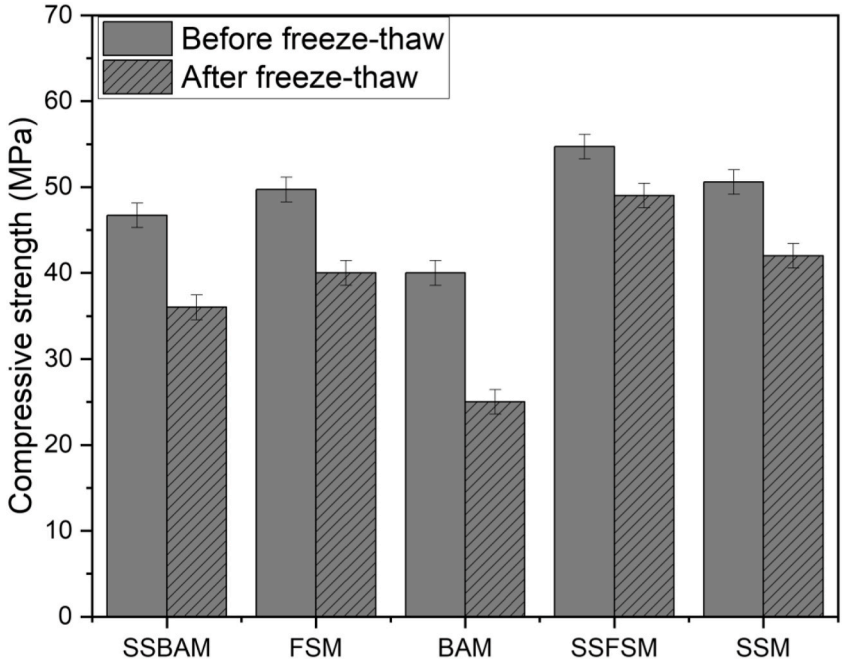

Fig. 12. Compressive strength of mortars before and after exposure to freeze-thaw.

makes BAM less resistant to the freeze-thaw effect and water ingress, resulting in physical deterioration and detachment of the mortar components. In addition, FSM had comparable mass and strength loss to SSM. As observed in the UPV results in Section 3.4.2, FSM had comparable porosity to SSM, as indicated by their UPV values. Conversely, lower mass and strength loss was observed in SSBAM than in BAM, ascribed to its higher UPV values (see Section 3.4.2) and better microstructural compactness (see Section 3.2.1). This indicates that SS has a beneficial effect on the mortar microstructure, resulting in enhanced frost resistance, lower mass loss, and higher residual strength. The presence of SS in the SSBAM mortar is presumed to have lowered the penetration of water and reduced the amount of freezable water throughout the mortar microstructure, which in turn lowered the internal damage and microcrack propagation due to the greater internal hydraulic stress caused by the volume expansion of frozen water. Meanwhile, the lowest mass loss and highest residual strength observed in SSFSM could be ascribed to the incorporation of a mix of FS and SS aggregates, which resulted in better particle packing, lower porosity, higher pore refinement, and microstructural compactness, as indicated by its higher UPV and lower capillary water absorption value. The use of a mix of FS and SS is believed to have lowered the effect of freeze-thaw action and the ingress and movement of water into the mortar microstructure, thus providing higher mitigating capacity for internal damage and better resistance to freeze-thaw conditions than the remaining samples.

3.5.4. Freeze-thaw in a combined sulfate and chloride solution

During the winter in Northern Europe, most roads and surrounding areas are treated with salt to melt the ice and prevent slippery roads. Therefore, the climatic conditions in the Nordic countries require mortars and concrete to have resistance properties to freeze-thaw, deicing salt, and marine conditions, particularly when they are used as outdoor materials and exposed to these conditions. Fig. 13 shows the visual appearance of all mortar samples after exposure to freeze-thaw in a combined sulfate and chloride solution. After exposure, the FSM and BAM mortars were destroyed, whereas the SSM, SSFSM, and SSBAM samples remained stable but had slight patches around their edges. The complete deterioration of FSM and BAM may be due to the volume expansion of absorbed solutions in their pores due to the dual effect of freeze-thaw and combined sulfate and chloride attack. The high stability of SSM, SSFSM, and SSBAM may be attributed to their compact microstructure, which resists the freeze-thaw effect and lowers the solution penetration. These observations demonstrate the superior resistance of SSM, SSFSM, and SSBAM samples to degradation in aggressive environments compared with FSM and BAM samples.

The mass loss and residual compressive strength of the samples due to exposure to freeze-thaw conditions in combined sulfate and chloride solutions are presented in Figs. 14 and 15. All samples exhibited mass loss and strength reduction after exposure, except for FSM and BAM, which could not be measured due to complete deterioration. The mass losses of SSM, SSFSM, and SSBAM after exposure were 3%, 5%, and 4.5%, respectively, while the compressive strength losses of SSM, SSFSM, and SSBAM after exposure were 31%, 40%, and 39%, respectively. Out of all the samples, SSM exhibited the lowest mass loss and highest residual strength and hence higher resistance to freeze-thaw in combined sulfate and chloride attack than the other samples. This may be because SS contains crystalline quartz, which is less susceptible to sulfate and chloride attacks. Meanwhile, the mass loss and reduction in strength of all samples were attributed to simultaneous exposure to freeze-thaw cycles and combined chloride and sulfate solutions, which can significantly amplify the degree of freeze-thaw damage. The ingress and transportation of sulfate and chloride ions into the mortar microstructure can cause

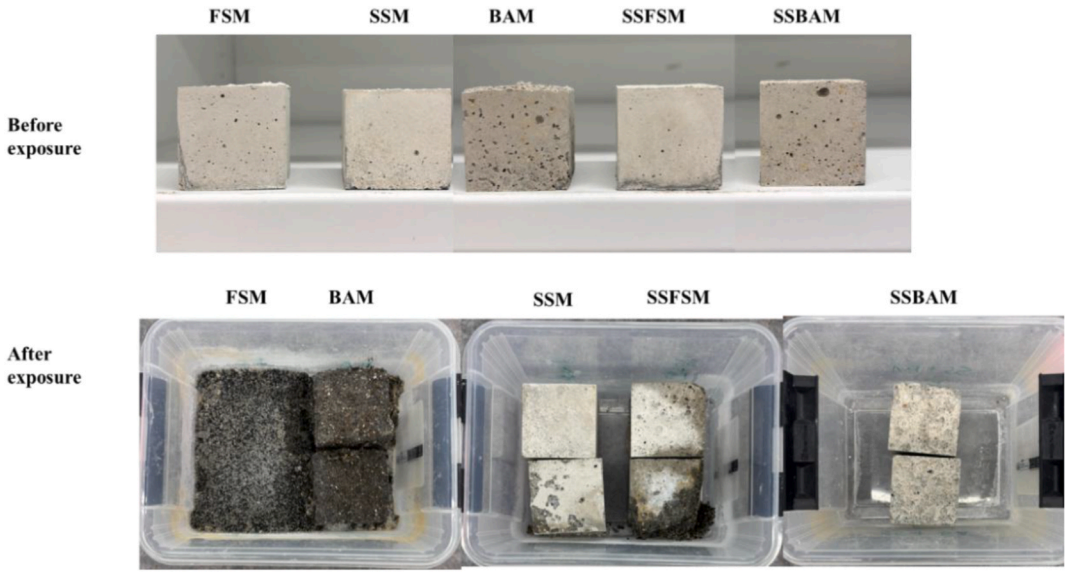

Fig. 13. Visual observation of mortar samples after exposure to freeze-thaw in combined sulfate and chloride solutions.

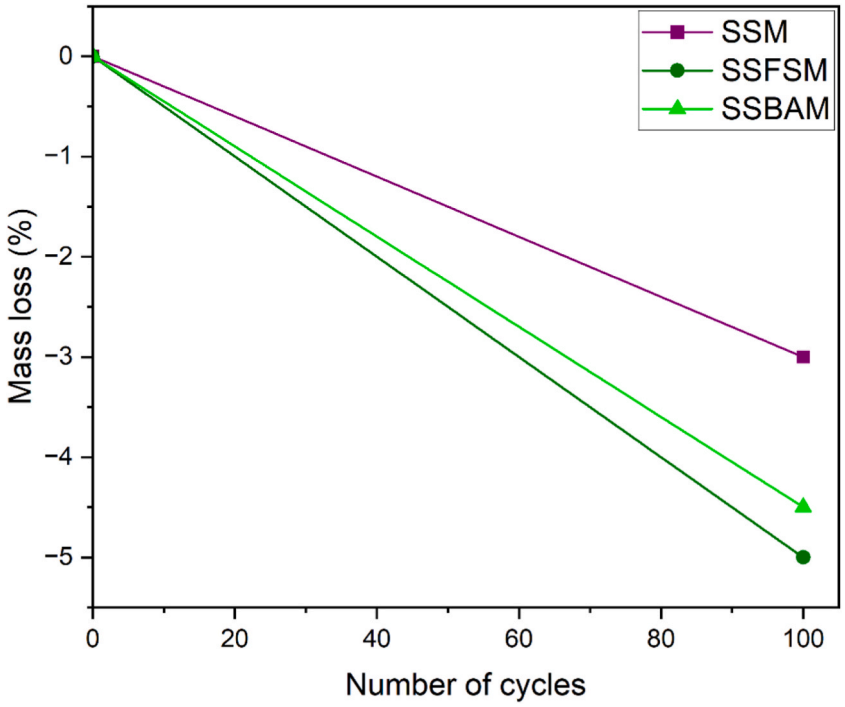

Fig. 14. Mass loss of mortar samples due to freeze-thaw exposure in combined sulfate and chloride solutions.

chemical volume changes in the material due to the reaction between the sulfate and chloride ions and the cementitious materials. The chemical reaction of chloride and sulfate ions with mortar components such as calcium hydroxide, AFm, or unreacted C_3A under freeze-thaw conditions can result in the rapid production of expansive agents (ettringite, gypsum, and Friedel's salt), leading to spalling, crack propagation, reduction in mechanical properties, and sometimes eventual collapse of the mortar.

4. Conclusions

This study investigated the feasibility of upcycling FS and municipal solid waste incineration BA as alternative fine aggregates in

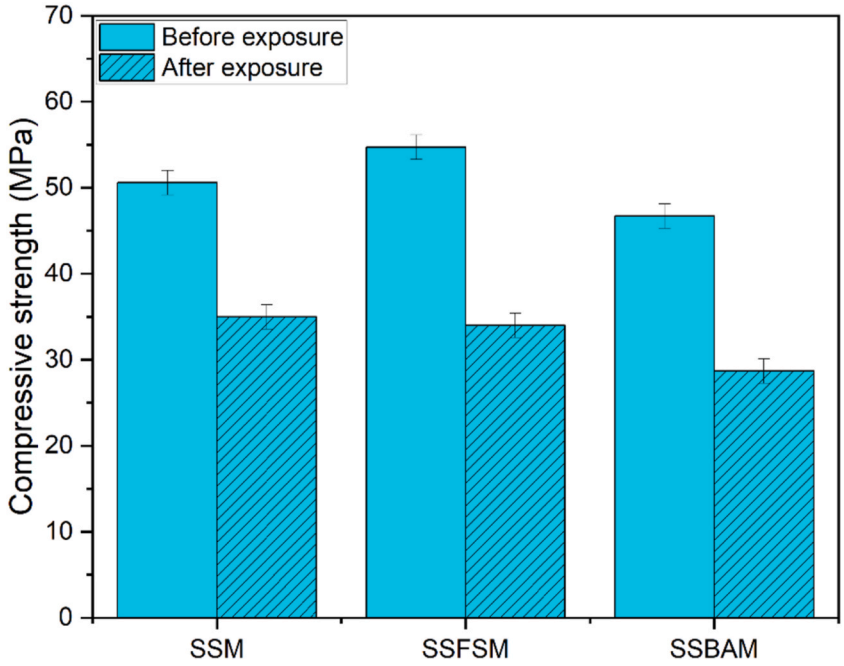

Fig. 15. Compressive strength of the mortar samples before and after exposure to freeze-thaw in combined sulfate and chloride solutions.

cement mortar production for potential construction applications. The FS used in this study was an industrial residue from nickel refining processes, whereas the BA was an industrial residue from the municipal solid waste incineration process. The upcycling of FS and BA as sand replacements in cement mortar production complies with the concept of zero waste and sustainability. By doing so, landfilling costs could be avoided, and the environmental impact and volume of natural aggregates needed to produce mortars could be reduced. SS was used as the reference aggregate. The effect of replacing SS wholly or partially with either FS or BA was investigated through workability, compressive strength, UPV, SEM analysis, capillary water absorption, ASR, freeze-thaw cycles in water, and combined sodium sulfate and sodium chloride solution exposure. The leaching test results revealed that FS and BA were environmentally friendly and suitable for use as sand replacements in cement mortar development. However, the experimental results showed that differences in aggregate properties exist, which influenced the fresh, hardened and durability properties of the mortars. For instance, SS is round with a smooth surface, whereas FS is angular and irregular in shape with a rough texture. In contrast, BA is irregular and angular in shape with a porous texture. Partial or total replacement of SS with FS or BA resulted in lower workability compared with the reference mortar. The total replacement of SS with FS resulted in comparable strength, UPV, and capillary water absorption, whereas the partial replacement of SS with FS resulted in higher strength, UPV, and lower capillary water absorption compared with the reference mortar. Furthermore, partial or total replacement of SS with BA resulted in lower compressive strength, UPV, and higher capillary water absorption compared with the reference mortar. The compressive strength of all samples after 28 days was above 20 MPa, satisfying the minimum compressive strength requirement for building bricks subjected to severe weathering in accordance with the ASTM C62 standard. In addition, after 28 days, the UPV values of all the mortar samples were above 3700 m/s and can therefore be classified as good mixes. As indicated by the ASTM C1260 standard, FS satisfies the ASR limit requirements with the lowest expansion rate at 14 and 28 days, indicating nonreactive behavior. All remaining aggregates had expansion rates above the ASR limit at 14 and 28 days, except for a mix of SS and FS, which had an expansion rate of 0.16% below the limit at 28 days. All samples remained stable after exposure to freeze-thaw cycles in water regardless of the aggregate type. However, the mortar samples containing a mix of SS and FS aggregates exhibited higher stability than the other samples, which can be attributed to their denser and compact microstructure. All the samples were destroyed after exposure to freeze-thaw in combined sulfate and chloride solution, except for reference samples and samples containing 50% replacement of SS with either FS or BA, which remained stable. Overall, this study contributes to understanding the suitability of using FS and BA as fine aggregates and their influence on cement mortars' physical, mechanical, microstructural, and durability properties. However, despite demonstrating the potential and suitability of FS and BA as sand replacements in cement mortar, this study has some limitations that require further investigation. The life cycle assessment and environmental impact of using these materials as eco-friendly alternatives remain largely unknown. Future research directions include life cycle analysis, cost–benefit analysis, and pilot-scale production.

CRediT authorship contribution statement

Adeolu Adediran: Writing – review & editing, Writing – original draft, Visualization, Validation, Supervision, Methodology, Investigation, Funding acquisition, Formal analysis, Conceptualization. **Nana Asaam:** Writing – review & editing, Writing – original

draft, Visualization, Validation, Investigation, Formal analysis, Conceptualization. **Javier Manso-Morato:** Writing – review & editing, Writing – original draft, Visualization, Methodology, Investigation, Formal analysis, Conceptualization. **Erdi Avci:** Writing – review & editing, Writing – original draft, Visualization, Validation, Methodology, Investigation, Formal analysis, Conceptualization. **Priyadharshini Perumal:** Writing – review & editing, Writing – original draft, Visualization, Validation, Methodology, Investigation, Formal analysis, Conceptualization.

Declaration of competing interest

The authors declare the following financial interests/personal relationships which may be considered as potential competing interests:Priyadharshini Perumal reports financial support was provided by Interreg Europe. Adeolu Adediran reports financial support was provided by Finnish Cultural Foundation. If there are other authors, they declare that they have no known competing financial interests or personal relationships that could have appeared to influence the work reported in this paper.

Acknowledgements

This work was done as part of Ar2CorD project (NPA0100039) funded by Interreg Northern Periphery and Arctic. Adeolu Adediran gratefully acknowledges funding from Finnish Cultural Foundation for his postdoctoral research. The authors gratefully acknowledge the Centre for Material Analysis, University of Oulu, Finland for assistance with data analysis.

Appendix A. Supplementary data

Supplementary data to this article can be found online at https://doi.org/10.1016/j.jobe.2026.116374.

Data availability

Data will be made available on request.

References

[1] A. Adediran, T. Van Truong, P. Perumal, Novel non-conventional raw materials as supplementary cementitious materials for low-carbon composite cement: chemical reactivity, fresh and hardened state characterization, Environ. Res. 271 (2025) 121146, https://doi.org/10.1016/j.envres.2025.121146.
[2] A. Adediran, M. Rajczakowska, A. Steelandt, I. Novakova, A. Cwirzen, P. Perumal, Conventional and potential alternative non-conventional raw materials available in Nordic countries for low-carbon concrete: a review, J. Build. Eng. 104 (2025) 112384, https://doi.org/10.1016/j.jobe.2025.112384.
[3] P.N. Lemougna, S. Gouda, A. Adediran, V. Isteri, P. Tanskanen, K. Kilpimaa, Recycling analcime residues of lithium production from spodumene ore in eco-friendly cementitious binders, Case Stud. Constr. Mater. 22 (2025) e04556, https://doi.org/10.1016/j.cscm.2025.e04556.
[4] A. Adediran, J. Yliniemi, S. Moukannaa, D.D. Ramteke, P. Perumal, M. Illikainen, Enhancing the thermal stability of alkali-activated Fe-rich fayalite slag-based mortars by incorporating ladle and blast furnace slags: physical, mechanical and structural changes, Cement Concr. Res. 166 (2023) 107098, https://doi.org/10.1016/j.cemconres.2023.107098.
[5] A. Adediran, J. Yliniemi, V. Carvelli, E. Adesanya, M. Illikainen, Durability of alkali-activated Fe-rich fayalite slag-based mortars subjected to different environmental conditions, Cement Concr. Res. 162 (2022) 106984, https://doi.org/10.1016/j.cemconres.2022.106984.
[6] A. Adediran, J. Yliniemi, P.N. Lemougna, P. Perumal, M. Illikainen, Recycling high volume Fe-rich fayalite slag in blended alkali-activated materials: effect of ladle and blast furnace slags on the fresh and hardened state properties, J. Build. Eng. 63 (2023) 105436, https://doi.org/10.1016/j.jobe.2022.105436.
[7] T.-P. Huynh, S.-H. Ngo, Waste incineration bottom ash as a fine aggregate in mortar: an assessment of engineering properties, durability, and microstructure, J. Build. Eng. 52 (2022) 104446, https://doi.org/10.1016/j.jobe.2022.104446.
[8] A. Adediran, N. Asaam, J. Manso-Morato, P. Perumal, Low-carbon composite cement mortar incorporating local raw materials as SCMs: performance and life cycle analysis, J. Am. Ceram. Soc. 109 (2026) e70717, https://doi.org/10.1111/jace.70717.
[9] A. Adediran, J. Yliniemi, M. Illikainen, Development of sustainable alkali-activated mortars using Fe-Rich fayalitic slag as the sole solid precursor, Front. Built. Environ 7 (2021) 39, https://doi.org/10.3389/fbuil.2021.653466.
[10] A. Adediran, J. Yliniemi, M. Illikainen, Mineralogy and glass content of Fe-rich fayalite slag size fractions and their effect on alkali activation and leaching of heavy metals, Int. J. Ceram. Eng. Sci 3 (2021) 287–300, https://doi.org/10.1002/ces2.10107.
[11] K.S. Al-Jabri, A.H. Al-Saidy, R. Taha, Effect of copper slag as a fine aggregate on the properties of cement mortars and concrete, Constr. Build. Mater. 25 (2011) 933–938, https://doi.org/10.1016/j.conbuildmat.2010.06.090.
[12] C. Shi, C. Meyer, A. Behnood, Utilization of copper slag in cement and concrete, Resour. Conserv. Recycl. 52 (2008) 1115–1120, https://doi.org/10.1016/j.resconrec.2008.06.008.
[13] K.S. Al-Jabri, M. Hisada, S.K. Al-Oraimi, A.H. Al-Saidy, Copper slag as sand replacement for high performance concrete, Cement Concr. Compos. 31 (2009) 483–488, https://doi.org/10.1016/j.cemconcomp.2009.04.007.
[14] S.K.PInstitute Of Technology E. A, S. D. Doss, N. S, G.R, Partial replacement of copper slag as fine aggregate, Int. J. Civ. Eng. 4 (2017) 18–23, https://doi.org/10.14445/23488352/IJCE-V4I3P105.
[15] B. Gorai, R.K. Jana, Premchand, Characteristics and utilisation of copper slag—a review, Resour. Conserv. Recycl. 39 (2003) 299–313, https://doi.org/10.1016/S0921-3449(02)00171-4.
[16] M. Velumani, S. Gowtham, M.P. Dhananjayan, G. Tamil Eniyan, Strength assessment of concrete with copper slag as fine aggregates, Mater. Today Proc. (2023), https://doi.org/10.1016/j.matpr.2023.05.700.
[17] B.H.J. Pushpakumara, P.M.K.N. Bandara, Evaluating the effectiveness of copper slag waste as a fine aggregate in concrete, Constr. Build. Mater. 475 (2025) 141046, https://doi.org/10.1016/j.conbuildmat.2025.141046.
[18] M. Manjunatha, T.V. Reshma, K.V.G.D. Balaji, A. Bharath, R.B. Tangadagi, The sustainable use of waste copper slag in concrete: an experimental research, Mater. Today Proc. 47 (2021) 3645–3653, https://doi.org/10.1016/j.matpr.2021.01.261.
[19] M. Sridharan, T.Ch Madhavi, Investigating the influence of copper slag on the mechanical behaviour of concrete, Mater. Today Proc. 46 (2021) 3225–3232, https://doi.org/10.1016/j.matpr.2020.11.195.

[20] P.S. Ambily, C. Umarani, K. Ravisankar, P.R. Prem, B.H. Bharatkumar, N.R. Iyer, Studies on ultra high performance concrete incorporating copper slag as fine aggregate, Constr. Build. Mater. 77 (2015) 233–240, https://doi.org/10.1016/j.conbuildmat.2014.12.092.
[21] M. Velumani, A. Nirmalkumar, Feasibility Studies of Copper Slag as Fine Aggregate Replacement in Concrete, 2014.
[22] B. Patnaik, An experimental investigation on optimum usage of copper slag as fine aggregate in copper slag admixed concrete, Int. J. Curr. Eng. Technol 4 (2011) 3646–3648, https://doi.org/10.14741/Ijcet/4.5.2014.102.
[23] L.A. Sormunen, P. Kolisoja, Mechanical properties of recovered municipal solid waste incineration bottom ash: the influence of ageing and changes in moisture content, Road Mater. Pavement Des. 19 (2018) 252–270, https://doi.org/10.1080/14680629.2016.1251960.
[24] A. Adediran, S.M. Kikky, S.K. Adhikary, V. Ducman, P. Perumal, Upcycling municipal solid waste incineration bottom ash in clay-bonded bricks, Ceram. Int. 51 (2025) 8941–8954, https://doi.org/10.1016/j.ceramint.2024.12.324.
[25] L.A. Sormunen, A. Kalliainen, P. Kolisoja, R. Rantsi, Combining mineral fractions of recovered MSWI bottom ash: improvement for utilization in civil engineering structures, Waste Biomass Valor. 8 (2017) 1467–1478, https://doi.org/10.1007/s12649-016-9656-4.
[26] C.J. Spreadbury, M. McVay, S.J. Laux, T.G. Townsend, A field-scale evaluation of municipal solid waste incineration bottom ash as a road base material: considerations for reuse practices, Resour. Conserv. Recycl. 168 (2021) 105264, https://doi.org/10.1016/j.resconrec.2020.105264.
[27] A. Vaitkus, J. Grazulyte, V. Vorobjovas, O. Šernas, R. Kleiziene, Potential of MSWI bottom ash to be used as aggregate in road building materials, Baltic J. Road Bridge Eng. 13 (2018) 77–86, https://doi.org/10.3846/bjrbe.2018.401.
[28] K. Polozhiy, M. Keppert, M. Jogl, R. Černý, Mechanical behavior of the cement mortar with high amount of municipal solid waste incineration (MSWI) bottom ash as an alternative aggregate, Adv. Mater. Res. 982 (2014) 74–78, https://doi.org/10.4028/www.scientific.net/AMR.982.74.
[29] J. Gražulytė, A. Vaitkus, O. Šernas, L. Žalimienė, The impact of MSWI bottom ash as aggregate on concrete mechanical performance, Int. J. Pavement Eng. 23 (2022) 2903–2911, https://doi.org/10.1080/10298436.2021.1873333.
[30] A. Cheng, Effect of incinerator bottom ash properties on mechanical and pore size of blended cement mortars, Mater. Des. 36 (2012) 859–864, https://doi.org/10.1016/j.matdes.2011.05.003.
[31] P. Tang, M.V.A. Florea, P. Spiesz, H.J.H. Brouwers, Characteristics and application potential of municipal solid waste incineration (MSWI) bottom ashes from two waste-to-energy plants, Constr. Build. Mater. 83 (2015) 77–94, https://doi.org/10.1016/j.conbuildmat.2015.02.033.
[32] Q. Wang, H. Chu, F. Li, Incorporating incineration bottom ash in environmentally friendly ultra-high performance concrete: impact on mechanical properties, durability, and environmental benefits, Constr. Build. Mater. 481 (2025) 141640, https://doi.org/10.1016/j.conbuildmat.2025.141640.
[33] Q. Wang, H. Chu, J. Jiang, B. Zhu, Enhancing mechanical performance and durability of high strength mortar with incineration bottom ash via Al2O3 micro-powder: an experimental study, J. Build. Eng. 89 (2024) 109268, https://doi.org/10.1016/j.jobe.2024.109268.
[34] H. Chu, Q. Wang, W. Zhang, Optimizing ecological ultra-high performance concrete prepared with incineration bottom ash: utilization of Al2O3 micro powder for improved mechanical properties and durability, Constr. Build. Mater. 426 (2024) 136152, https://doi.org/10.1016/j.conbuildmat.2024.136152.
[35] H. Li, H. Chu, Q. Wang, J. Tang, Feasibility of producing eco-friendly self-compacting mortar with municipal solid waste incineration bottom ash: a preliminary study, Case Stud. Constr. Mater. 19 (2023) e02309, https://doi.org/10.1016/j.cscm.2023.e02309.
[36] EN 196-1, Methods of Testing Cement. Part 1: Determination of Strength, European Committee for standardization, Brussels, 2016.
[37] SFS-EN 1097-5, SFS-EN 1097-5, tests for mechanical and physical properties of aggregates. Part 5: determination of the water content by drying in a ventilated oven. https://online.sfs.fi/fi/index/tuotteet/SFS/CEN/ID2/1/106043.html.stx, 2008. (Accessed 10 April 2026).
[38] SFS EN 1097-6, Tests for Mechanical and Physical Properties of Aggregates. Part 6: Determination of Particle Density and Water Absorption, 2014.
[39] EN 197-1, EN 197-1 Cement, Part 1: composition, quality requirements and conformity of common cements. https://online.sfs.fi/fi/index/tuotteet/SFS/CEN/ID2/1/182891.html.stx, 2011. (Accessed 16 August 2019).
[40] SFS-EN 12457-2, Characterisation of waste, Leaching. Compliance test for leaching of granular waste materials and sludges. One Stage Batch Test at a Liquid to Solid Ratio of 10 l/kg for Materials with Particle Size Below 4 Mm (Without or with Size Reduction), 2002.
[41] EN 1015-3, Methods of test for mortar for masonry, Determination of Consistence of Fresh Mortar (By Flow Table), European Committee for Standardization, 1999, p. 1999.
[42] Standard Test Method for Ultrasonic Pulse Velocity Through Concrete, ASTM International, West Conshohocken, PA, USA, 2022. Www.Astm.Org. (Accessed 13 April 2026). https://store.astm.org/c0597-22.html, 2022.
[43] ASTM C1585-20 - Standard Test Method for Measurement of Rate of Absorption of Water by Hydraulic-Cement Concretes, ASTM West, Conshohocken Pa. U. S, 2020, 2020, https://standards.iteh.ai/catalog/standards/astm/9f8fba0a-739f-43a3-bd10-71060497a92c/astm-c1585-20. (Accessed 16 July 2025).
[44] ASTM C666/C666M - 15 Standard Test Method for Resistance of Concrete to Rapid Freezing and Thawing, ASTM International, West Conshohocken, PA, USA, 2015, p. 2015. Www.Astm.Org. (Accessed 3 January 2017). https://www.astm.org/Standards/C666.htm.
[45] Standard Test Method for Potential Alkali Reactivity of Aggregates (Mortar-Bar Method), ASTM International, West Conshohocken, PA, USA, 2023. Www.Astm.Org. (Accessed 13 April 2026). https://store.astm.org/c1260-23.html, 2023.
[46] FINLEX, Finlex ® - translations of Finnish acts and decrees: 843/2017 English. https://www.finlex.fi/en/laki/kaannokset/2017/en20170843, 2017. (Accessed 22 March 2021).
[47] European Commission, Directive 2008/98/EC on waste (waste framework directive) - environment - european commission. http://ec.europa.eu/environment/waste/framework/, 2008. (Accessed 29 November 2018).
[48] T. Zhang, Z. Zhao, Optimal use of MSWI bottom ash in concrete, Int. J. Concr. Struct. Mater. 8 (2014) 173–182, https://doi.org/10.1007/s40069-014-0073-4.
[49] A.A. Al-Rawas, A. Wahid Hago, R. Taha, K. Al-Kharousi, Use of incinerator ash as a replacement for cement and sand in cement mortars, Build. Environ. 40 (2005) 1261–1266, https://doi.org/10.1016/j.buildenv.2004.10.009.
[50] M. De Schepper, P. Verlé, I. Van Driessche, N. De Belie, Use of secondary slags in completely recyclable concrete, J. Mater. Civ. Eng. 27 (2015) 04014177, https://doi.org/10.1061/(ASCE)MT.1943-5533.0001133.
[51] M. Mavroulidou, Mechanical properties and durability of concrete with water cooled copper slag aggregate, Waste Biomass Valor. 8 (2017) 1841–1854, https://doi.org/10.1007/s12649-016-9819-3.
[52] J. Yao, H. Song, Y. Li, Y. Cui, M. Chai, W. Ling, Mechanism of macro- and microscopic performance of cement mortars influenced by municipal solid waste incineration bottom ash as sand substitution, Constr. Build. Mater. 397 (2023) 132317, https://doi.org/10.1016/j.conbuildmat.2023.132317.
[53] M.R. Irshidat, N. Al-Nuaimi, M. Rabie, Potential utilization of municipal solid waste incineration ashes as sand replacement for developing sustainable cementitious binder, Constr. Build. Mater. 312 (2021) 125488, https://doi.org/10.1016/j.conbuildmat.2021.125488.
[54] R. Kurtulus, A. Adediran, C. Kurtulus, O. Mankinen, G. Almisned, H.O. Tekin, P. Perumal, J. Yliniemi, Fabrication and characterization of alkali-activated Fe-rich fayalitic slag as a sustainable radiation shielding material, Radiat. Phys. Chem. 235 (2025) 112885, https://doi.org/10.1016/j.radphyschem.2025.112885.
[55] M. Khanzadi, A. Behnood, Mechanical properties of high-strength concrete incorporating copper slag as coarse aggregate, Constr. Build. Mater. 23 (2009) 2183–2188, https://doi.org/10.1016/j.conbuildmat.2008.12.005.
[56] ASTM C62, ASTM C62-23, Standard Specification for Building Brick (Solid Masonry Units Made from Clay or Shale), 2023.
[57] A. Alzaza, K. Ohenoja, F.U. Ahmed Shaikh, M. Illikainen, Mechanical and durability properties of C–S–H-seeded cement mortar cured at fluctuating low temperatures with granulated blast furnace slag as fine aggregates, J. Build. Eng. 57 (2022) 104879, https://doi.org/10.1016/j.jobe.2022.104879.
[58] J.R. Leslie, abd W.J. Cheesman, An ultrasonic method of deterioration and cracking in concrete structures, ACI. J. Proc 46 (1949), https://doi.org/10.14359/12041.
[59] H. Jin, S. Ghazizadeh, J.L. Provis, Thermodynamic modelling of alkali-silica reactions in blended cements, Cement Concr. Res. 181 (2024) 107543, https://doi.org/10.1016/j.cemconres.2024.107543.
[60] M. Bagheri, B. Lothenbach, K. Scrivener, The effect of paste composition, aggregate mineralogy and temperature on the pore solution composition and the extent of ASR expansion, Mater. Struct. 55 (2022) 192, https://doi.org/10.1617/s11527-022-02015-6.
[61] Š. Šachlová, A. Kucharová, Z. Pertold, R. Přikryl, Evaluation of alkali–silica reaction potential of quartz-rich rocks by alkaline etching of polished rock sections, Environ. Earth Sci. 75 (2016) 730, https://doi.org/10.1007/s12665-016-5519-3.

[62] M. Shakoorioskooie, M. Griffa, A. Leemann, R. Zboray, P. Lura, Alkali-silica reaction products and cracks: X-ray micro-tomography-based analysis of their spatial-temporal evolution at a mesoscale, Cement Concr. Res. 150 (2021) 106593, https://doi.org/10.1016/j.cemconres.2021.106593.
[63] E.R. Gallyamov, A. Leemann, B. Lothenbach, J.-F. Molinari, Predicting damage in aggregates due to the volume increase of the alkali-silica reaction products, Cement Concr. Res. 154 (2022) 106744, https://doi.org/10.1016/j.cemconres.2022.106744.
[64] U. Müller, K. Rübner, The microstructure of concrete made with municipal waste incinerator bottom ash as an aggregate component, Cement Concr. Res. 36 (2006) 1434–1443, https://doi.org/10.1016/j.cemconres.2006.03.023.
[65] M.L. Schafer, K.A. Clavier, T.G. Townsend, C.C. Ferraro, J.M. Paris, B.E. Watts, Use of coal fly ash or glass pozzolan addition as a mitigation tool for Alkali-silica reactivity in cement mortars amended with recycled municipal solid waste incinerator bottom ash, Waste Biomass Valor. 10 (2019) 2733–2744, https://doi.org/10.1007/s12649-018-0296-8.
[66] S. Abbas, U. Arshad, W. Abbass, M.L. Nehdi, A. Ahmed, Recycling untreated coal bottom ash with added value for mitigating alkali–silica reaction in concrete: a sustainable approach, Sustainability 12 (2020) 10631, https://doi.org/10.3390/su122410631.
[67] N. Holmes, H. O'Malley, P. Cribbin, H. Mullen, G. Keane, Performance of masonry blocks containing different proportions of incinator bottom ash, Sustain. Mater. Technol. 8 (2016) 14–19, https://doi.org/10.1016/j.susmat.2016.05.001.
[68] A. Adediran, N. Asaam, P.N. Lemougna, P. Perumal, Reuse of volcanic material as a mineral additive in spodumene tailings-based ceramic production: physical, mechanical, structural, and durability changes, Chem. Eng. J. 526 (2025) 170874, https://doi.org/10.1016/j.cej.2025.170874.